Modeling Line-Commutated Converter HVDC Transmission Systems Using Dynamic Phasors

By

Mehdi Daryabak

A thesis submitted to the Faculty of Graduate Studies
in partial fulfilment of the requirements for the degree of
Doctor of Philosophy

Department of Electrical and Computer Engineering
Faculty of Engineering
University of Manitoba
Winnipeg, Manitoba

April 2016

Abstract

This thesis develops the dynamic phasor model of a line-commutated converter (LCC) high-voltage direct current (HVDC) transmission system. The mathematical definition and properties of dynamic phasors are utilized to model both the dc-side and the ac-side of a LCC-HVDC transmission system as well as 6-pulse Graetz bridge, which is the building block of such a system.

The developed model includes low-frequency dynamics of the systems, i.e., fundamental frequency component (50 Hz) at the ac-side and dc component at the dc-side, and removes high-frequency transients. The developed model, however, is capable of accommodating higher harmonics if necessary. The model is also able to simulate the system during abnormal modes of operations such as unbalanced operation and commutation failure. In order to develop the dynamic phasor model of a line-commutated converter, the concept of switching functions is utilized.

The developed model is capable of capturing large-signal transients of the system as well as steady state operating conditions. The model can be used in order to decrease the computational intensity of LCC-HVDC simulations. The developed model in this thesis enables the user to consider each harmonic component individually; this selective view of the components of the system response is not possible to achieve in conventional electromagnetic transient simulations.

Contents

List of Tables

List of Figures

Chapter 1

Introduction

1.1 Background

High-voltage direct current (HVDC) transmission systems play an integral role in modern electric power networks. HVDC is considered to be a suitable option for such applications as:

- *transmission via underground/submarine cables;*

  In such cases conventional transmission via high-voltage ac lines will face major operating challenges posed by the excessive capacitance of the underground/submarine cables, whereas the direct-current nature of an HVDC system will not be impacted by the capacitance of the cable.

- *linking ac systems with unequal frequencies;*

  In cases where two or more ac electric networks with different frequencies (e.g., 50 Hz and 60 Hz) are to be connected, HVDC transmission systems are the only choice to do so.

- *long-distance transmission* [1], [2].

  Transmission of electric power over long distances with ac electric networks is limited by the amount of line reactance. Therefore, in order to overcome this problem and to utilize the full capacity of the transmission system, ac lines must be equipped with series/shunt compensators to reduce the total reactance. Series compensated lines may impose stability problems to the network, which need further investigation. On the other hand, the line reactance is not of concern in HVDC transmission systems as the voltages and currents are dc.

Although a new breed of HVDC systems using voltage-source converters (VSC) is also developed and is the subject of wide-spread interest, the majority of existing HVDC systems are based upon conventional line-commutated converters (LCC). LCC-HVDC schemes offer the benefits of a more mature technology (than the VSC-based systems) and are available in much larger ratings than the currently available VSC-HVDC systems. Presently, VSC-HVDC systems exist in power ratings of up to 1500 MW (per converter), whereas LCC-HVDC converters of more than twice this rating are commonly available [3]. Therefore, it is anticipated that LCC-HVDC systems will continue to play a major role in the future adoption of HVDC transmission.

The complexity of interconnected power systems disallows an extended use of analytical methods for their design. Limitations of field experiments (in terms of feasibility of experiments and security of the grid), on the other hand, often render them infeasible for practical purposes to analyze the behaviour of the network. Therefore, computer simulations for modeling, analysis, design, and operation of power systems have been the practice of choice over the past few decades since the advent of modern computing platforms.

Power system transient simulation programs are broadly categorized to two types [4]:

- Electromagnetic transient (EMT) programs;
- Electromechanical transient programs.

Electromagnetic transient programs are the most accurate type of computer simulation programs for simulating transients in an electric power network. EMT simulators are historically used for the study of short-term, fast transients, which typically include frequencies that exceed the fundamental; they use detailed models and numerically demanding solution methods, which make them computationally affordable only for small networks or studies with a short period of interest.

On the other hand, electromechanical transient programs have been developed to study slower dynamics, which involve oscillations of machine rotors and typically include frequencies less than the fundamental. These types of programs are also called transient stability programs. The period of interest in transient stability programs is longer than EMT-type studies, ranging from a few seconds to several tens of minutes. Electromagnetic transient simulation programs, in which high-fidelity models of transmission systems and power electronic converters are available, have been extensively used for the analysis and design of HVDC schemes. For instance, in [5] the authors investigate the modeling and simulation of the first CIGRE HVDC benchmark system using two simulation tools, namely the PSCAD/EMTDC and PSB/SIMULINK, and compare the results. In [6] a procedure for using optimization-enabled electromagnetic transient simulation for the design of HVDC system controls is introduced. In this work a sequence of simulation runs of the network are conducted, which are guided by a nonlinear optimization algorithm. In [7] an electromagnetic transient program-based study of the CIGRE HVDC benchmark system operating with weak ac systems is carried out.

Despite the accuracy of an EMT simulator in representing fast transients within HVDC systems, an EMT simulator may indeed be excessively detailed for the study of large, interconnected networks with embedded HVDC, particularly when only the low-frequency dynamics of the network are of interest. For such cases simulation of the switching transients, which are often small in magnitude, adds unnecessary computational complexity and prolongs the simulation time. This problem becomes exacerbated in modern power grids wherein multiple HVDC converters may converge in close electrical proximity in schemes known as multi-infeed HVDC [8]. Multi-infeed systems are known to give rise to complex and interacting transients [9], which render modeling with conventional EMT simulators computationally inefficient.

This research presents a computationally low-cost, average-value model for an LCC-HVDC system using dynamic phasors. Dynamic phasors use the quasi-periodic switching nature of a power electronic converter, for which voltages and currents can be represented using time-varying Fourier coefficients [4], [10], [11]. Dynamic phasor modeling retains the low-frequency dynamic characteristics of a power system without having to model the high-frequency transients caused by the operation of power-electronic switches and converters. Additionally, a dynamic phasor model can be easily augmented to account for harmonic components, if so needed.

Dynamic phasors have been successfully used in modeling and analysis of electrical machines [12], [13], [14], power system dynamics and faults [15], [16] flexible ac transmission systems (FACTS) devices [17], [18] sub-synchronous resonance (SSR) [19], dc-dc converters [20], multi-converter dc systems [21], multi-converter ac systems [22], and renewable energy systems [23]. Special studies including real-time and repetitive simulations [24], [6], [25] can benefit from the reduction in computational intensity offered by dynamic phasor modeling. A dynamic phasor model of a line-commutated converter has been developed in [26], however the authors use a different approach to derive the model, which is valid only for the fundamental frequency component under balanced operating conditions. The developed model in this research uses the switching functions of the converter voltages and currents, which enable one to include higher harmonic components if so needed. In addition, the developed model can properly model the large-signal dynamics of LCC-HVDC transmission systems operating under unbalanced conditions as well as during commutation period.

1.2 Research Objectives and Motivation

This research extends the use of dynamic phasors to modeling of large-excursion transients of LCC-HVDC transmission systems, caused by control actions or faults. The reduced simulation intensity of the model resulting from its neglecting switching transients makes it particularly useful in the study of large-signal, low-frequency transients, or in repetitive simulations when time savings over conventional EMT simulations become significant. The objectives and motivation of this thesis are as follows.

1. *Dynamic phasor modelling of LCC-HVDC transmission systems*;

   A dynamic phasor-based model of the line-commutated converter is derived based on the switching functions that are described in Chapter 3. In addition, dynamic phasor models of the ac network, transmission line (π model), and phase locked loop (PLL) will also be derived.

2. *Inclusion of higher harmonics;*

   The developed model can include higher harmonic orders as well as the fundamental frequency component. As an example the 11^{th} and 13^{th} order harmonics are added to the ac current of an LCC to clearly show the effect of including higher order harmonics.

3. *Commutation failure;*

   The developed model from (2) above is not able to properly simulate the behaviour of the system during transients in which commutation failure occurs. Therefore, modifications are needed in order to accurately model the system during these transients.

4. *Operating under unbalanced conditions;*

   The models to be developed (2) and (3) require modifications in order to be able to properly simulate the system operating under unbalanced conditions. The results are shown for various unbalanced conditions including unbalanced faults at the converter bus.

The dynamic phasor models are developed in MATLAB and the results are compared against those obtained from the PSCAD/EMTDC, which is a widely used electromagnetic transient simulator. The results of PSCAD/EMTDC are accurate and they are well matched with experimental results. Therefore, comparing the results of the developed dynamic phasor model against the results of the PSCAD/EMTDC is considered to be a reasonable and convincing test to conclude that the developed models work properly.

One of the main advantages of modeling using dynamic phasors over electromagnetic transient simulations is its ability to include or exclude various portions of the system response (in terms of frequency contents) in the simulations in favour of a simplified and computationally more affordable model. As an example in the modeling of LCC-HVDC, it is possible to add any combinations of harmonic orders to the simulations. For example, the user may choose to only include the 13^{th} order harmonic and not the 11^{th} to solely focus on a single harmonic content. The same can be said for unbalanced terms. The separated components can be much more insightful to the system designer, which can use them for various purposes including controller design. On the other hand, the electromagnetic transient simulations produce the most detailed and accurate results without much information about the effects of various terms.

1.3 Thesis Organization

Chapter 2 discusses various types of transient simulation programs in power systems including electromagnetic and electromechanical transient simulations. After that the description of the mathematical foundations of modeling using dynamic phasors is provided.

In Chapter 3, the basic operation of an LCC-HVDC transmission system for both the power circuit and the control systems are discussed and the governing steady state and dynamic equations of the line-commutated converter are derived.

In Chapter 4, a dynamic phasor-based model for the CIGRE HVDC benchmark model [27] is developed using MATLAB/SIMULINK. The chapter will proceed with the definition of the switching functions and development of the dynamic phasor model of the line-commutated converter, dc system, ac network, and phase-locked loop (PLL).

The developed average-value dynamic phasor model is validated against a detailed switching model implemented in PSCAD/EMTDC. In order to investigate the accuracy of the dynamic phasor model in representing transient events, a third model of the system is also developed used, in which the bridge converters are modeled with dynamic phasors, while the ac system is represented using a constant admittance matrix.

In Chapter 5, the dynamic phasor model of the LCC-HVDC transmission system developed in Chapter 4 is extended to simulate the system under unbalanced conditions as well as during commutation failure periods.

In Chapter 6, the conclusions and contributions of this research are discussed and a number of directions for work are proposed for further investigation on this subject.

Chapter 2

Power System Transient Simulation

2.1 Overview of Power System Transient Simulation

Due to the complexity and interconnectivity of large power networks, use of analytical methods for their control, design, operation, and maintenance is extremely challenging if not impossible altogether. Therefore, computer simulation of power systems has been used over the past decades for these purposes.

There are various types of studies that need to be conducted for a power system each involving different components, different portions of the network, and different time-periods of interest. The frequency of interest in power system studies varies from fractions of 1 Hz up to several MHz depending on the types and objectives of studies. Figure 2-1 illustrates the various types of power system transient studies and their corresponding frequencies of interest [28].

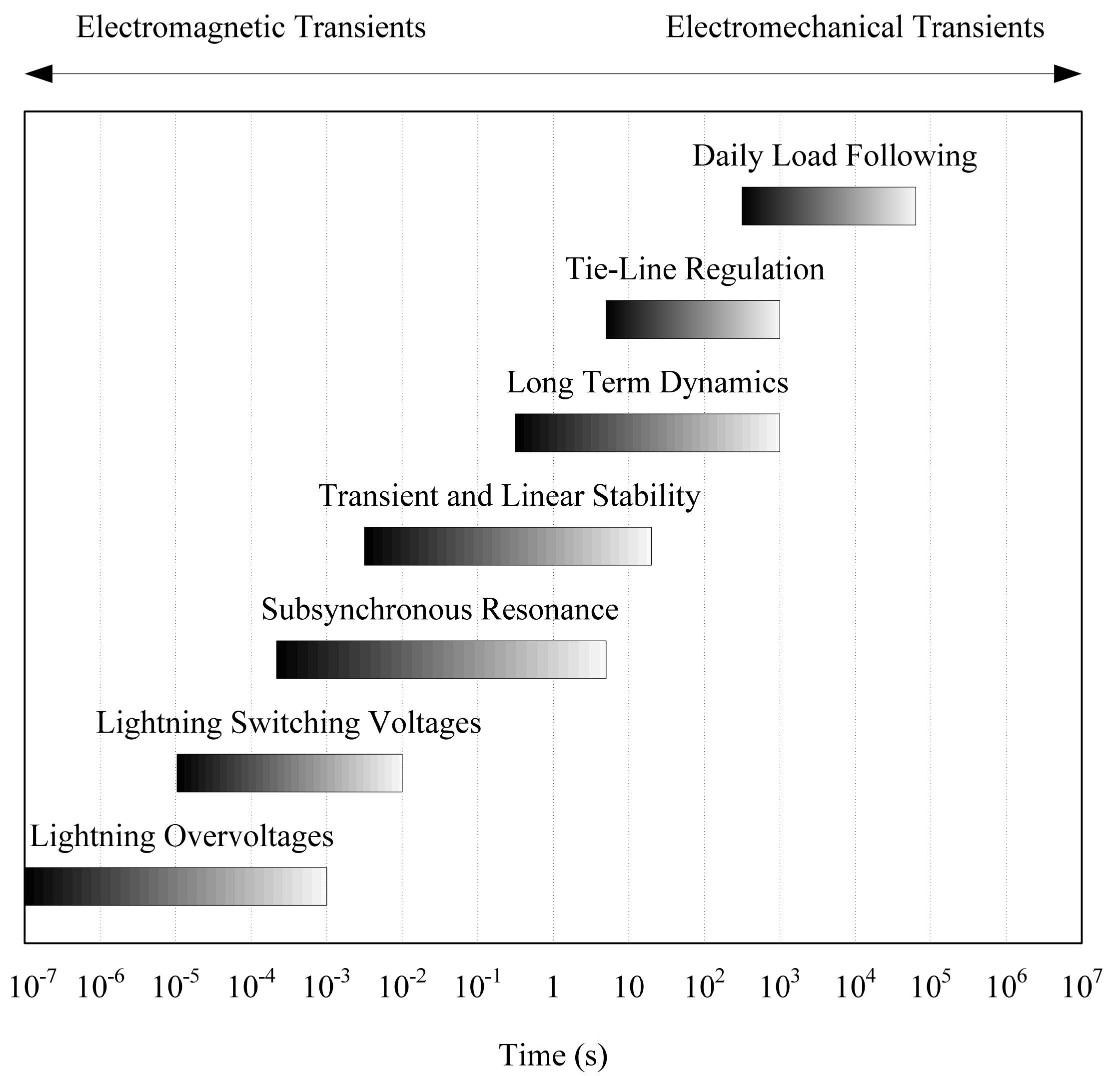

Figure 2-1: Time scale of power system transients.

In power system simulations if the frequency range of interest is high, i.e., when a transient phenomenon with rapid variations is to be studied, detailed and accurate models of components and a small simulation time step have to be used in order to properly simulate the network. The models need to contain adequate details to allow representation of the transient phenomenon. If such a study must be done for a large network, then the simulation becomes slow and computationally expensive, or at times even impossible, to perform.

On the other hand, in the studies where the frequency range of interest is low, models with less detail and large simulation time-steps suffice, and simulations for large networks are computationally affordable. Decisions regarding the accuracy of models and solution methods, and the trade-off between accuracy and computational complexity of the resulting simulation need to be made for a study of transients in power systems.

2.2 Electromagnetic Transient Simulation

Electromagnetic transient (EMT) programs are the most accurate and detailed type of power system transient simulation programs. Component models used in EMT programs contain a large level of details.

EMT programs are most suitable for the study of fast transients (usually more than nominal steady state frequency). SF6 transients [29], wave propagation [30], lightning transients [31], switching over-voltages [32], insulation coordination [33], transformer saturation [34], HVDC systems [6], and design of flexible ac transmission systems (FACTS) [35] are examples of studies commonly done with EMT programs.

EMT programs use small time-steps (typically in the order of a few micro-seconds) to properly simulate fast transients. As a rule of thumb, the time step in an EMT program needs to be at least one-tenth to one-fiftieth of the minimum of the smallest time constant and the smallest oscillation period in the system for proper simulation of transient events. Therefore, EMT simulators are suitable choices only for the studies with a small network or studies with a short period of interest. Otherwise, the resulting simulation becomes too slow and sometimes even impossible to conduct.

2.3 Electromechanical Transients Simulation

Unlike EMT simulators, electromechanical transient programs are most suitable for slower transients (usually less than nominal steady state frequency) in power systems. Sub-synchronous resonance [36], transient stability (rotor dynamics) [37], inertia oscillations [38], mid-term, and long-term stability [39] are some of the studies that are done commonly with electromechanical transient programs. The period of interest for electromechanical transients is usually between a few seconds to tens of minutes. For this reason, simplified models of power system components are used; otherwise the simulations become too slow and sometimes even impossible to perform.

Electromechanical transient programs use a quasi-steady state approach to modeling and simulation, which allows them to use large step sizes upwards of tens of milli-seconds. In electromechanical transient simulations it is often assumed that the frequency of the electrical network remains constant at the rated, which then allows representation of the ac systems using simplified phasor models. Although this assumption is valid for low-frequency transients, it becomes increasingly inaccurate in the presence of fast-acting and high-frequency system components such as LCC-HVDC.

In an LCC-HVDC transmission system if the dc current of the converter is assumed to be purely dc, i.e., comprising only one component with a 0 Hz frequency, the fundamental component of the ac line current will be a sine wave with a fixed amplitude and with a frequency of f_s (nominal frequency of the electric network, e.g., 50 Hz or 60 Hz). However, during transients the dc current may undergo oscillations and hence will not be constant. If the dc current, during its transient variations, has a low-frequency oscillatory component at f_o, it can be shown that the amplitude of the fundamental component of the ac line current will have oscillations at f_o. This amplitude-modulated fundamental component results in two sidebands of $f_s + f_o$ and $f_s - f_o$ [40]. If f_o is relatively small (typically below 5 Hz) both sidebands are adequately close to f_s and the ac system may be represented using a constant admittance representation (also called a phasor model). However, if f_o is large both sidebands differ significantly from f_s and the constant-frequency assumption of the electric network in no longer acceptable. Therefore, a simulation program based upon the assumption of a constant-frequency ac system cannot properly simulate the transient events.

As discussed above, both the electromagnetic and the electromechanical transient simulations have their own merits and disadvantages. There is a gap between these two methods of power system simulations, which needs to be filled. A new method of power system simulations is required in such cases where a relatively large electric network needs to be simulated while the dynamics of the ac or dc power system cannot be accurately modeled with the assumption of constant frequency for the (ac) network. The dynamic phasors method for power system simulation is proposed to overcome the difficulties associated with electromagnetic and electromechanical transient simulation.

2.4 Modeling Using Dynamic Phasors

2.4.1 Definitions

A firm understanding of the concept of dynamic phasors and the way they are applied to modeling dynamic systems is essential in creating a model using them. The following section presents a description of dynamic phasors.

The concept of dynamic phasors is based on the generalized averaging method proposed in [10]. Consider a waveform $x(\tau)$ viewed over the interval $\tau \in (t-T,t]$; the waveform can be described using its Fourier series expansion coefficients $\langle x \rangle_k(t)$ as follows.

$$x(t-T+s) = \sum_{k=-\infty}^{\infty} \langle x \rangle_k (t)\, e^{jk\omega_s (t-T+s)} \tag{2-1}$$

where $s \in [0,T]$, $\omega_s = 2\pi/T$, and the coefficients are obtained as follows.

$$\langle x \rangle_k (t) = \frac{1}{T}\int_0^T x(t-T+s)\, e^{-jk\omega_s (t-T+s)} ds \tag{2-2}$$

In modeling power electronic converters T is selected to be the switching period. The notation $\langle x \rangle_k(t)$ describes the k^{th} order harmonic component. In the simulation of power system transients, $x(\tau)$ may be any arbitrary voltage or current waveform within the circuit.

The waveform $x(\tau)$ may contain a variety of harmonic components. For example, the dc-side voltage waveform of a 6-pulse LCC converter contains a large dc (i.e., 0-order) component as well as $6n$ harmonics. The ac current of the same converter contains a large fundamental (k = 1) components as well harmonic components of the orders $6n \pm 1$.

Although the waveform $x(\tau)$ may attain periodicity in steady state, it may not generally repeat the same form in each switching period during transients. As such its Fourier coefficients over the interval $(t\text{-}T,t]$ will not be constant when t is allowed to slide; they will rather be functions of time and hence the notation $\langle x\rangle_k(t)$. These coefficients are referred to as *dynamic phasors*. In the other words, dynamic phasors are the complex Fourier coefficients of the waveform $x(t)$.

The benefit of this generalized averaging approach is in enabling its user to select a desired number of Fourier coefficients to construct an approximation of the original waveform. For example, if the waveform $x(\tau)$ comprises both low- and high-frequency components, the user may choose to only consider its low-frequency contents in a simplified representation. Normally only the first or the first few dominant harmonic components are selected for this purpose. Inclusion of additional components increases the accuracy of estimation at the expense of a higher-order model, which will naturally translate to computationally more demanding simulations (due to the requirement of smaller time-steps).

2.4.2 Mathematical properties of dynamic phasors

When applying dynamic phasors to model power system components, the following properties prove useful.

$$\left\langle \frac{dx}{dt} \right\rangle_k (t) = \frac{d}{dt}\langle x\rangle_k (t) + jk\omega_s \langle x\rangle_k (t) \tag{2-3}$$

$$\langle xy\rangle_k (t) = \sum_{i=-\infty}^{\infty} \langle x\rangle_{k-i}(t)\langle y\rangle_i (t) \tag{2-4}$$

$$\langle x \rangle_{-k} = \langle x \rangle_k^* \tag{2-5}$$

where * denotes the complex conjugate operator. Equation (2-5) is valid only if $x(\tau)$ is a real function.

Equation (2-3) holds for situations where the fundamental frequency ω_s is constant. It is shown in [10] that the same formulation remains largely accurate when the system frequency changes, in particular when the rate of change of frequency is slow. In the work presented in this thesis the frequency is not assumed to change drastically. Therefore the equation (2-3) remains accurate.

The fundamental operations presented in this section are used in Chapter 3 to build models for different blocks of an LCC-HVDC system, which are then interfaced to form its average model.

2.5 State-of-the-Art of Simulation of Electrical Networks Using Dynamic Phasors

A great deal of work has been done by many authors to solve the dynamic phasor equations of electrical networks. In [4], the author uses the example described below to compare the dynamic phasor method of solving power system equations with electromagnetic and electromechanical transient simulations. In this example assume a contingency in the electrical network, which may cause the frequency of the system to deviate by 2% (i.e., variations between 58.8 Hz and 61.2 Hz in a 60 Hz system). In some severe contingencies the frequency can deviate up to 10%. Now assuming that 20 steps per cycle provides accurate results, one needs to use the simulation time step of 0.8 ms ((1/60)/20 = 0.00083 s).

On the other hand, in the dynamic phasor-based method the integration is done on a much slower waveform, which allows to the use of a larger time step. In that example it was shown that the 8.0 ms time step is enough to have accurate results, which can potentially make the simulation 10 times faster. Although the 8.0 ms time step is acceptable in most transient stability programs these programs assume that the frequency of the network is constant, which causes major inaccuracies in case the frequency of the network deviates by a considerable amount.

In [4], the author also uses the relaxed trapezoidal integration method and proposes a variable time step simulation to decrease the time step during a transient and then increase it as the simulation approaches steady state. In simulations using dynamic phasors the simulation time step can be very large in steady state because phasors become constants and there is no need for small time steps. The author also compares the accuracy and stability of several integration methods with each other.

In [41], the author uses the exponential method for numerical integration to discretize differential equations. The dynamic phasor equation of electrical components (resistor, capacitor, inductor, ...) and control systems are converted to the algebraic form in the branch level to create the network admittance matrix and solve it by nodal analysis method.

In [16], the author examines a number of integration methods and analyzes them in terms of numerical accuracy, stability and efficiency. The author also optimizes the integration methods for dynamic phasor equations.

As mentioned above, in the literature a voluminous amount of work has been done to show the efficiency, accuracy, and stability of dynamic phasors for simulation of electrical networks. The main purpose of the present research is to develop the dynamic phasor equations of LCC-HVDC transmission systems for both balanced and unbalanced conditions as well as during commutation failure. The specific numerical integration method for solving the derived equations is not the focus of this research. The derived state-space equations are implemented in MATLAB/SIMULINK and solved by one of MATLAB's internal ODE solvers.

2.6 Chapter Summary

This chapter provided a brief overview of the principles of transient simulation of power systems. Study of fast transients requires small time steps in order to properly simulate the phenomenon at hand. Therefore, simulation of fast transients is normally confined to small electrical networks in order to perform the simulation in a reasonable period of time and on available computing platforms. On the other hand, studies involving slower transients can be done on larger electrical networks, as simplified models of electrical components are used.

The dynamic phasors method for power system simulation has been proposed to retain the slower dynamics without having to model higher order transients. However, it is possible to add any number of harmonics if so desired. Dynamic phasors have the flexibility to adjust the level of representation to the needs of the study at hand.

In addition, dynamic phasors have the advantage of separating different terms in the simulations making the simulations more insightful. This can be helpful from various aspects including controller design and harmonic interaction studies.

Chapter 3

LCC-HVDC Transmission Systems

Figure 3-1 shows a schematic diagram of a 12-pulse mono-polar line-commutated converter-based high-voltage direct current (LCC-HVDC) transmission system. The system layout shown in this diagram is similar to the first CIGRE HVDC benchmark system [27] which is used as a case study in this research.

In the following sections a LCC-HVDC transmission system is briefly explained in terms of its ac systems, dc system, line-commutated converter, and control systems.

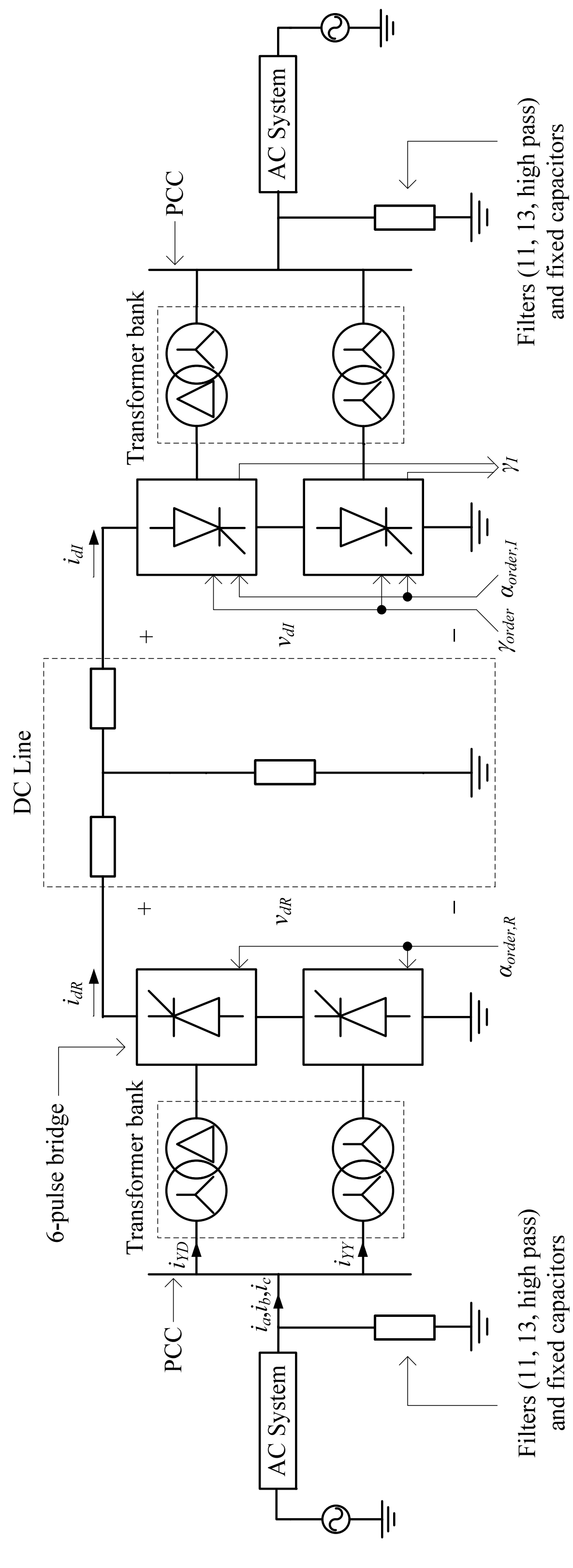

Figure 3-1: A 12-pulse LCC-HVDC transmission system.

3.1 AC Systems

The ac side of an HVDC transmission system for both the rectifier and the inverter includes an equivalent ac source, harmonic filters, and a transformer bank. In the case study that is described in this thesis the ac system is modeled with a Thevenin equivalent circuit. The ac system is often characterized with its short-circuit ratio (SCR).

The SCR is defined as the short-circuit capacity of ac converter bus divided by the active power of the converter. In HVDC applications, the effective short circuit ratio (ESCR) is used more often than the SCR. In calculating ESCR the effect of HVDC harmonic filters are also considered; the amount of reactive power produced by the filters are reduced from the short circuit capacity of the ac bus and then the result is divided by the dc power. Therefore, the ESCR value is less than the value of SCR. An ac system may be characterized as very weak system to a strong based on its ESCR value. Higher ESCRs generally mean a more robust ac systems and hence an easier control task. The following are the approximate ranges for weak and strong system designations based on ESCR [42].

$ESCR < 1.5$: Very weak system

$1.5 \leq ESCR < 2.5$: Weak system

$2.5 \leq ESCR < 5$: Strong system

3.1.1 AC filters

Filters are used to prevent penetration of current harmonics of the ac side of the converters to the network. Filters are designed to filter the lowest <u>dominant</u> harmonics (eleventh and thirteenth in case of a 12-pulse converter) [1]. There is also a high-pass filter for filtering higher order harmonics. Filters are also designed to provide the required reactive power for proper operation of the converters.

3.1.2 Transformers

A transformer bank is used to convert the voltage level of the ac system to a voltage level that is suitable for proper operation of the converters and the dc transmission line. The transformer bank in a 12-pulse converter configuration consists of a Y-Δ transformer and a Y-Y transformer, which results in elimination of the sixth order harmonic in each of the six-pulse converters. In this case the eleventh and the thirteenth order harmonics are the lowest two remaining harmonics, thereby resulting in filters with smaller size and lower cost.

3.2 Line-Commutated Converter

3.2.1 Principles of operation

Figure 3-2 shows a schematic diagram of a 6-pulse Graetz bridge, which is the building block of a LCC-HVDC transmission system. This converter block consists of six thyristor valves, which are fired consecutively (as numbered in Figure 3-2) with a delay of α (in radians) known as the firing angle measured with respect to a particular instant of time, which is most commonly selected to be the positive zero-crossing of the line voltage. The dc side of the converter is represented using a constant current source of $i_d \approx I_d$. In practice large smoothing reactors are deployed on the dc side of LCC-HVDC systems to ensure that the dc line current is essentially constant and with minimum ripple. On the ac side, the converter is connected to a set of three-phase voltages via transformers. For the analysis that follows a lossless converter is assumed, i.e., the switches do not incur losses during turn-on and turn-off periods and also have no losses during conduction.

Figure 3-3 shows the dc voltage and ac current waveforms of the LCC. It also includes the square and trapezoidal waveform approximations of the ac current that are discussed later in this chapter.

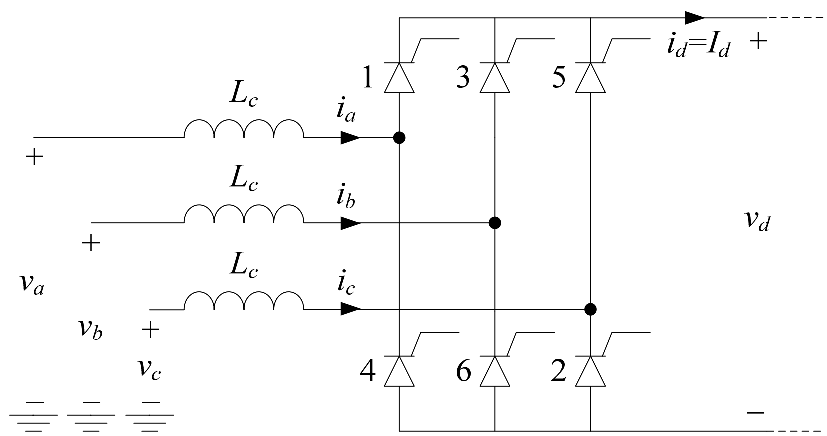

Figure 3-2: Circuit diagram of a line commutated converter (LCC).

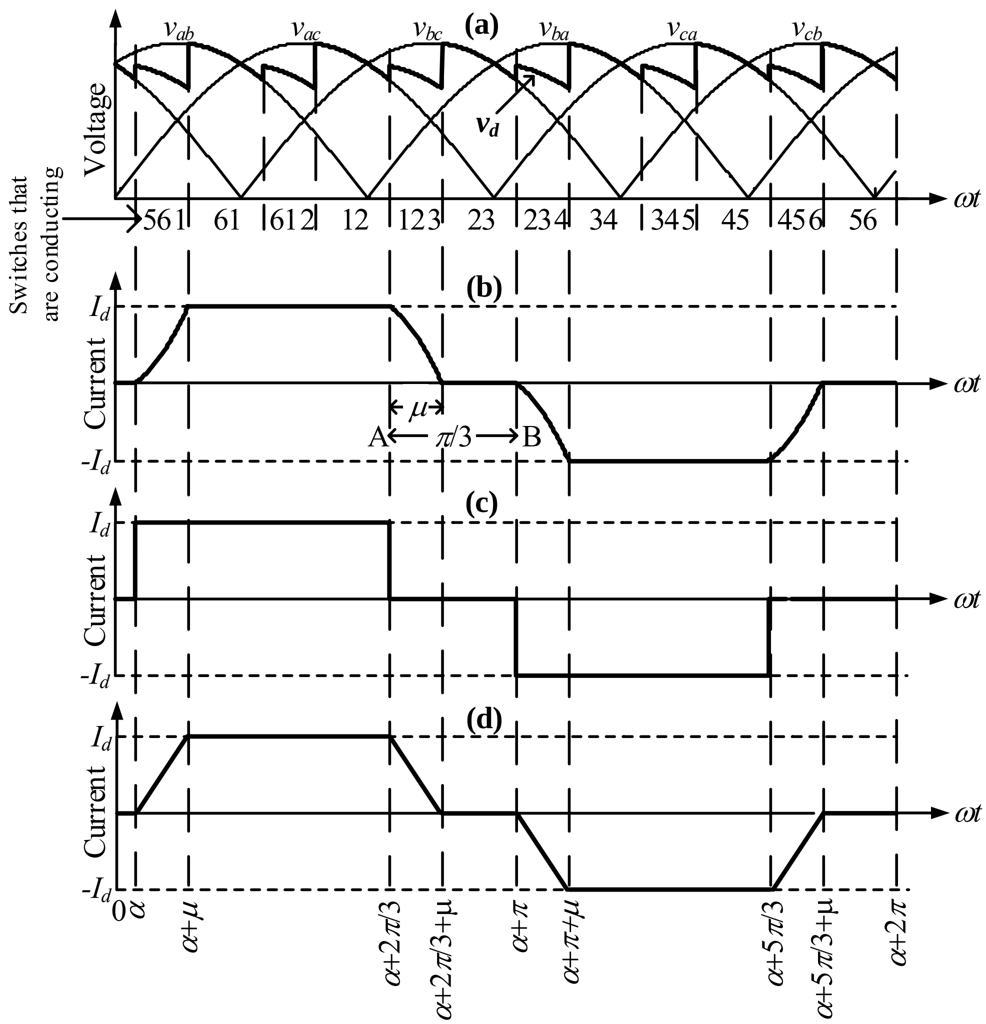

Figure 3-3: Line commutated converter waveforms. (a) three-phase line voltages and the dc voltage; (b) phase-a line current; (c) square-wave approximation of the ac line current;(d) trapezoidal approximation of the ac line current.

It is noted that the ac line current (Figure 3-3(b)) contains a finite duration of time over which the current moves from one constant value to another, e.g., from 0 to I_d or from I_d to 0. This period of time starts at the switching instant and has an angular duration of μ, and is widely known as the commutation period. The commutation period results from the ac-side inductance (L_c), which opposes an instantaneous transition between the current levels. The switches that are involved in the process of commutation will be ON during this period;

one switch will have diminishing current flow while the other one will gain increasing current. During the overlap period the ac line current has a nonlinear transition between its two constant boundary values as seen in Figure 3-3(b). The equivalent circuit of the LCC during commutation period between switches 1 and 5 is shown in Figure 3-4. The commutation period between other switches is similar under balanced operating conditions as long as operation conditions remain intact.

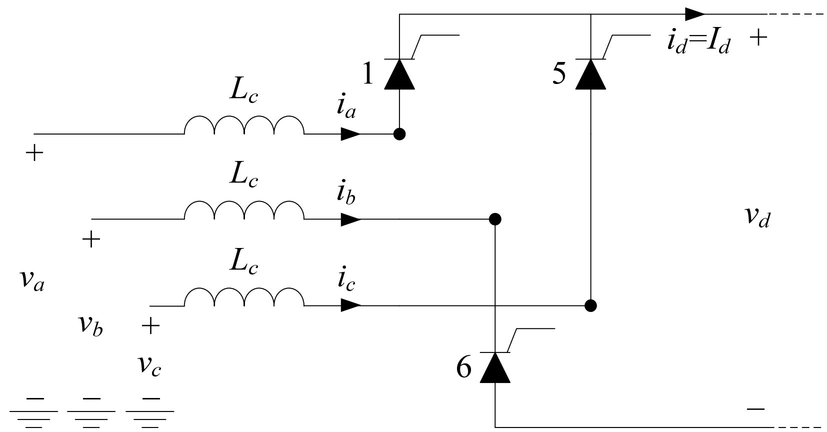

Figure 3-4: Equivalent circuit of the LCC during commutation between valves 1 and 5.

3.2.2 Waveform analysis

In the following, analytical expressions are developed for the actual ac line current.

It is assumed that the phase voltages of the ac system are balanced as follows.

$$\begin{cases} v_a = V_m \sin(\omega t + \pi / 6) \\ v_a = V_m \sin(\omega t - \pi / 2) \\ v_a = V_m \sin(\omega t + 5\pi / 6) \end{cases} \tag{3-1}$$

To find the phase-a current (i_a) during a given overlap period, e.g., between valves 1 and 5 when the dc voltage transfers from v_{cb} to v_{ab} as shown in Figure 3-4, the sets of equations in (4-22) must be solved.

$$\begin{cases} v_a - L_s \dfrac{di_a}{dt} = v_c - L_s \dfrac{di_c}{dt} \\ i_c = I_d - i_a \\ i_a(\omega t = \alpha) = 0 \\ i_a(\omega t = \alpha + \mu) = I_d \end{cases} \tag{3-2}$$

Solution of these equations results in the following expression for i_a.

$$i_a(\omega t) = I_s(\cos\alpha - \cos(\omega t)) \tag{3-3}$$

where

$$I_s = \frac{\sqrt{3}V_m}{2L_s\omega} \tag{3-4}$$

and V_m is the peak value of ac phase-voltage, L_s is the source-side inductance, and ω is the nominal angular frequency of the system. With this expression for the phase-a current during the given overlap interval, the following expression for i_a for the entire period can be obtained.

$$
i_a(\omega t)=\begin{cases}
I_s(\cos\alpha-\cos(\omega t)) & \alpha\le\omega t\le\alpha+\mu\\
I_d & \alpha+\mu\le\omega t\le\alpha+\frac{2\pi}{3}\\
I_d-I_s(\cos\alpha-\cos(\omega t-\frac{2\pi}{3})) & \alpha+\frac{2\pi}{3}\le\omega t\le\alpha+\frac{2\pi}{3}+\mu\\
0 & \alpha+\frac{2\pi}{3}+\mu\le\omega t\le\alpha+\pi\\
-I_s(\cos\alpha+\cos(\omega t)) & \alpha+\pi\le\omega t\le\alpha+\pi+\mu\\
-I_d & \alpha+\pi+\mu\le\omega t\le\alpha+\frac{5\pi}{3}\\
I_s(\cos\alpha+\cos(\omega t-\frac{2\pi}{3}))-I_d & \alpha+\frac{5\pi}{3}\le\omega t\le\alpha+\frac{5\pi}{3}+\mu\\
0 & \alpha+\frac{5\pi}{3}+\mu\le\omega t\le\alpha+2\pi
\end{cases}\tag{3-5}
$$

This representation for the ac line current proves to be overly complicated for its intended use in an analytical formulation of the converter operation using dynamic phasors; therefore, approximations are considered to simplify it. A square wave (see Fig. 3.3 (c)) is widely used to approximate the ac current waveform of an LCC [1]. To better represent the variations of the ac current during overlap periods, a trapezoidal approximation (see Fig. 3.3(d)) is also considered in this thesis. In the following section, the fundamental component of both the square-wave and the trapezoidal-wave approximations are compared with that of the above expression.

The power factor of the converter system resulting from the actual current waveform and its two approximations will also be studied. The aim of the next section is to investigate the amount of error that is introduced in the fundamental component of the line current and the converter's power factor as a result of square-wave and trapezoidal-wave approximations.

3.2.3 Waveform approximation for the AC current

As it can be seen from (4-22) the actual ac line current is excessively complicated to be used in dynamic phasor modeling method. Due to switching phenomena, the ac-side current of a line-commutated converter is not purely sinusoidal and its actual wave shape depends on such factors as the magnitude of the applied ac voltage, ac line inductance, dc-side current, firing angle (α), commutation period (μ), and frequency of the system as seen in (4-22). When LCC-HVDC systems are simulated using an electromagnetic transient (EMT) simulator, the ac line current waveform is represented with adequate accuracy provided that a small enough simulation time-step is selected. While it is possible to use the ac current waveform directly as in (3.5), these expressions are often found to be overly complicated due to the nonlinear transitions of the current during overlap periods. As such piecewise linear approximations of the ac current waveform are commonly used [1]. Dynamic phasor modeling of a LCC will also be much simplified with a piecewise linear approximation of the ac current waveform. The accuracy of the results of a study conducted using an approximation will depend on how faithful a simplified representation is in capturing the properties of the actual ac line current. It is therefore necessary to quantify the error introduced by approximate waveforms in the development of dynamic phasor models.

It should also be noted that including additional details in order to obtain more accurate results might not be always advantageous; this is because for the analysis of a system the uncertainty of a model's parameters is also a determining factor in deciding if a more accurate method of solving will indeed result in more accurate and meaningful results.

This section develops analytical expressions for both square-wave [26], [40] and trapezoidal-wave [43] approximations and presents an analysis of the error of these two common waveforms in representing the fundamental frequency component of the ac current and the power factor of the converter.

The two approximations of the ac line current are also shown in Figure 3-3. The square wave approximation (Figure 3-3(c)) ignores the overlap period and shows sudden jumps at the instant of switching. The trapezoidal approximation (Figure 3-3(d)), however, includes a period of time equal in length to the actual overlap period, during which the current is assumed to vary linearly between the two boundary values.

Derivation of the fundamental components of the square and trapezoidal waveforms is straightforward as will be shown later. Although it is possible to derive a closed form expression for the fundamental component of the actual ac current [44], it provides little practical value in dynamic phasor modeling.

A. Fundamental Frequency Component of AC Current

The peak value of the fundamental component of the square-wave approximation (Figure 3-3(c)) is obtained as follows.

$$I^{(1)} = \frac{2\sqrt{3}}{\pi} I_d \tag{3-6}$$

Similarly, the following expression is obtained for the peak value of the fundamental frequency component of the trapezoidal approximation.

$$I^{(1)} = \frac{2\sqrt{3}}{\pi} I_d \frac{\sin(\frac{\mu}{2})}{(\frac{\mu}{2})} \tag{3-7}$$

Figure 3-5 shows the variation of the fundamental component of the ac current versus the overlap angle (μ). For convenience of comparison, the y-axis is per-unitized by the dc current I_d. A family of curves is shown for $\alpha = 0$ and 60° (rectifier mode of operation) and for $\alpha = 120$ and 150° (inverter mode of operation). Although the overlap angle is a function of the firing angle, it is shown as an independent variable as its value can be adjusted by other parameters, e.g., the ac side inductance, dc current, and ac voltage.

The overlap angle cannot exceed 60° (note that it is for this kind of overlap where there are only two switches involved), as can be deduced from Figure 3-3(b) by observing the distance of $\pi/3$ between the two points A and B. This period encompasses the overlap angle and as such the largest attainable value for the μ is 60°, as indicated on the x-axis in Figure 3-5. Also note that $\alpha+\mu$ cannot exceed 180°; therefore, for every value of the firing angle the corresponding curve continues only until $\mu=180°-\alpha$ (only overlap between two switches are considered here).

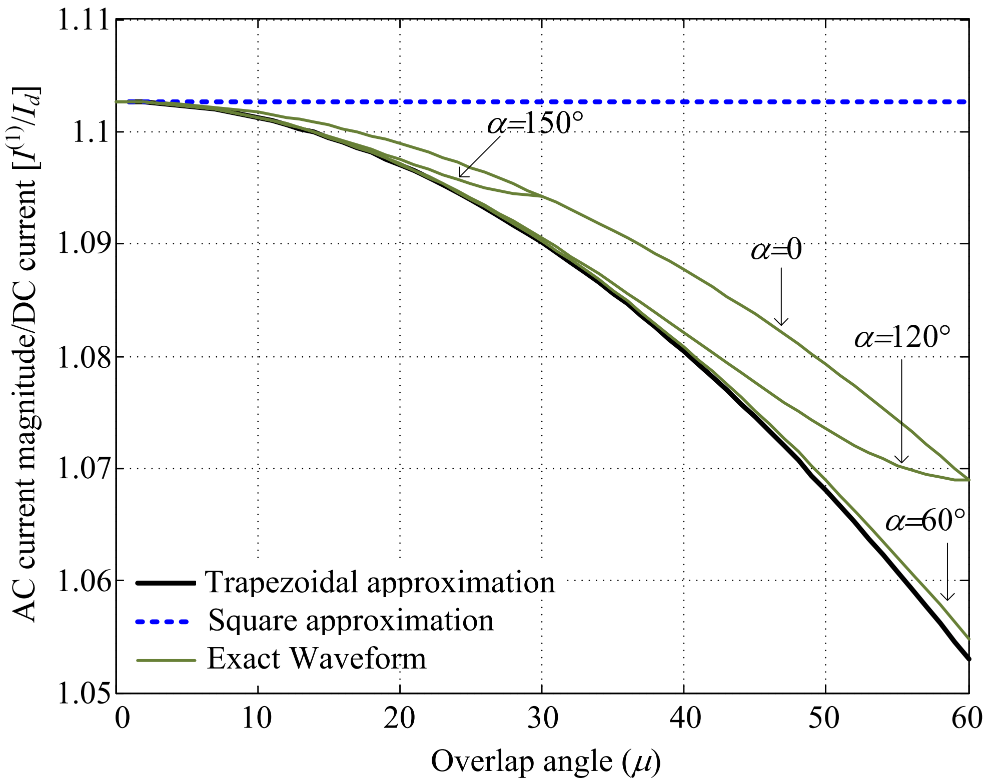

Figure 3-5: Fundamental frequency component of the ac current over dc current.

As shown in Figure 3-5, the square waveform approximation depends neither on the firing angle nor on the overlap angle and, therefore, has a constant value. The trapezoidal waveform, on the other hand, only depends on the overlap angle; the actual current waveform depends on both the firing angle and the overlap angle. As seen the approximate waveforms present varying degrees of error depending on the firing and overall angle combinations.

Figure 3-6 shows the calculated percentage error for the normalized fundamental frequency component of the ac current. Table 3-1 compares the maximum percentage errors for both approximate waveforms. As shown the largest absolute percentage error in estimating the fundamental component of the ac current is 4.54% for the square wave and

1.49% for the trapezoidal approximation, and both occur at μ=60°. In [1] the maximum percentage error of the square wave was reported as 4.3%, which is due to the division of the difference by the approximate value and not by the exact value as is done in this research.

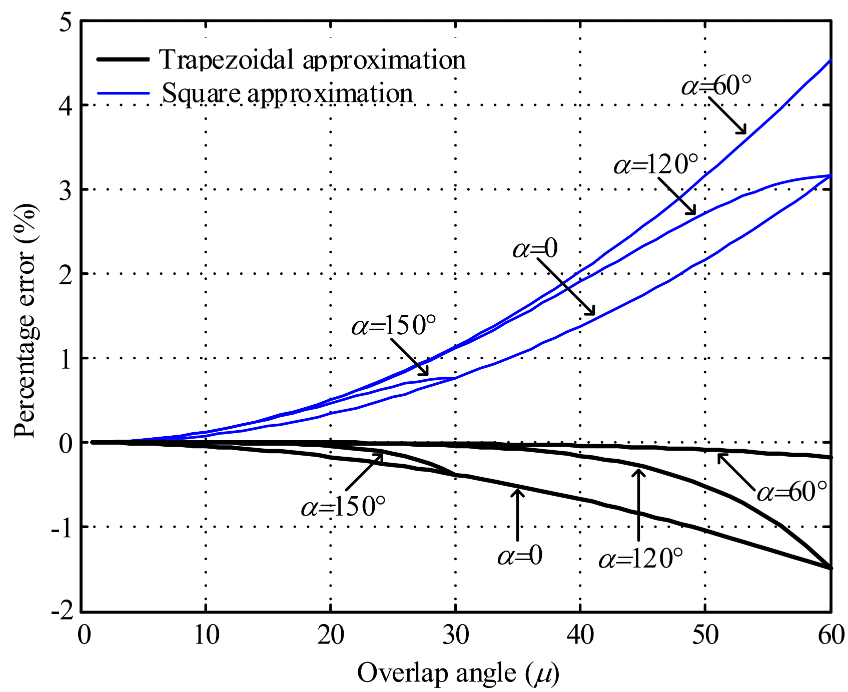

Figure 3-6: Percentage error of fundamental frequency component of ac current over dc current.

Table 3-1: Percentage error of both types of approximation

Max. percentage error of	Square approximation	Trapezoidal approximation
AC current magnitude	4.54	-1.49
AC current magnitude for normal operating condition (μ≤30°)	1.14	-0.38
Converter's power factor	-4.34	1.52
Converter's power factor for normal operating condition (μ≤30°)	-1.13	0.38

In practice the overlap angle is normally much smaller than 60° and hence the percentage error of the two approximations will be less. For example, for overlaps angles below 30° the square wave and the trapezoidal approximations will have percentage errors of less than 1.14% and 0.38%, respectively.

B. Converter Power Factor

For calculating the power factor of the converter it is assumed that the converter is lossless; i.e., the real power at its ac terminals equals the real power at its dc side. Therefore, the following expression can be stated.

$$3(\frac{V_m}{\sqrt{2}})(\frac{I^{(1)}}{\sqrt{2}}) \times \mathrm{PF} = V_d I_d \tag{3-8}$$

where V_d is the average dc voltage and is given in (4-22) [1], and PF is the power factor.

$$V_d = \frac{3\sqrt{3}}{\pi} V_m \cos\alpha - \frac{3}{\pi}\omega L_s I_d \tag{3-9}$$

From (3-9) the power factor of the converter is simply derived as follows.

$$\mathrm{PF} = \frac{2V_d I_d}{3V_m} \frac{1}{I^{(1)}} \tag{3-10}$$

As seen in (4-22) the approximation used for fundamental component of the ac current affects the calculation of the converter power factor. Therefore, the percentage error in estimating the converter's power factor is calculated for the two approximating waveforms. The results are shown in Figure 3-7 and the largest percentage errors are reported in Table 3-1. It is again seen that the trapezoidal approximation provides a much more accurate representation of the converter power factor.

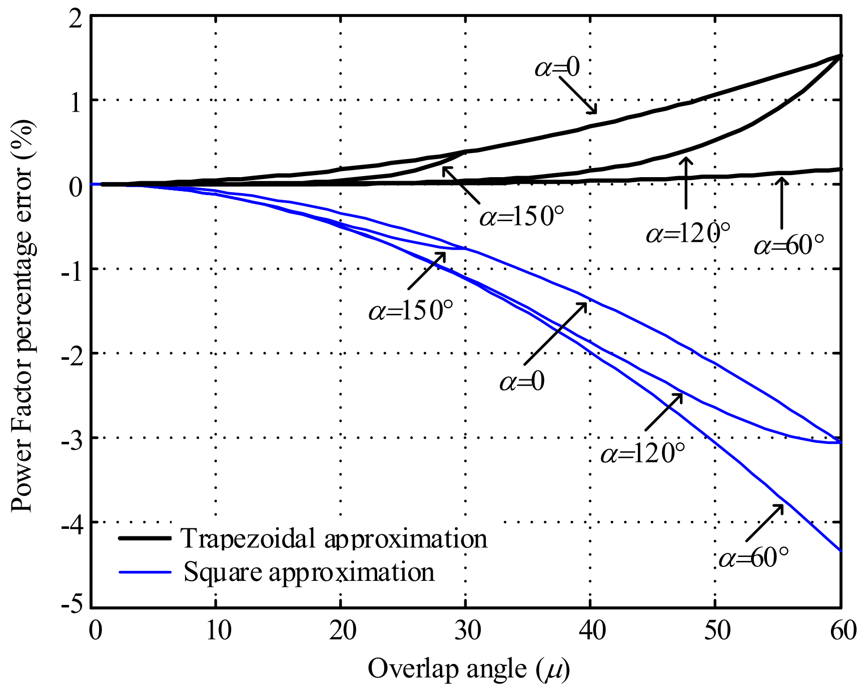

Figure 3-7: Percentage error of the power factor of the converter.

Based on the above results the trapezoidal approximation offers more accurate approximation than the square waveforms while the equations are still simple enough to be used in dynamic phasor method. Therefore, in this work the trapezoidal-wave approximation will be used.

3.3 Converter Control Systems

Figure 3-8 shows typical control blocks of a conventional LCC-HVDC system. The control variables used are also marked in Figure 3-1. Normally the rectifier controls the dc line current, whereas the inverter operates in constant extinction-angle control mode. Although additional control functions are deployed for special modes of operation, during normal operation the rectifier and inverter control functions can be described using proportional-integral (PI) controllers acting upon the dc current and the inverter extinction angle, respectively. The voltage-dependent current order limit (VDCOL) reduces the dc current-order during ac under-voltage conditions to protect the valves [1], [2], [6]. The internal components and connections used in the control system of Figure 3-8 are available in detail in [7] and [26] and are used in this thesis. To ensure proper timing of firing pulses to the converters phase-locked loops (PLLs) are employed at both ends. Modeling of the PLL is presented in the next chapter.

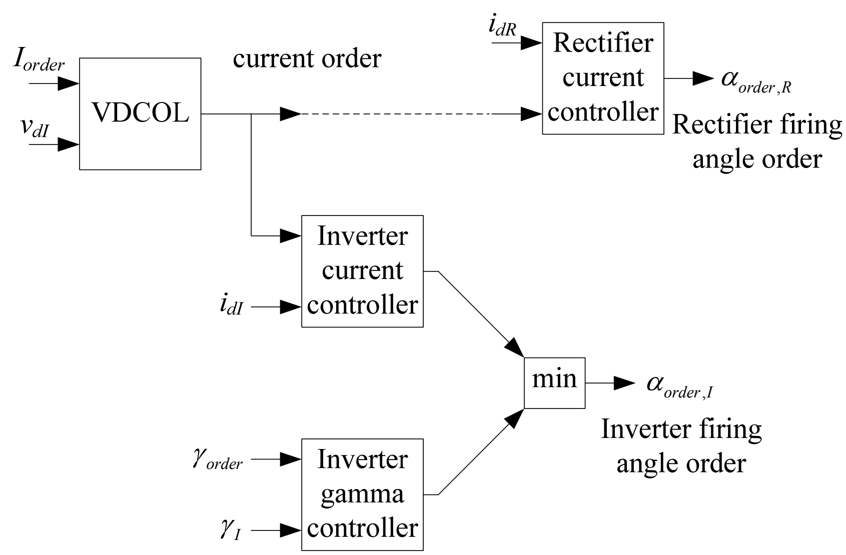

Figure 3-8: LCC-HVDC control scheme

3.4 Chapter Summary

In this chapter a brief introduction to a line-commutated converter based HVDC transmission system was presented. The various parts of a LCC-HVDC transmission system, such as ac systems, ac filters, transformers, line-commutated converter and control systems were also explained.

The rectangular and trapezoidal methods of approximation for the ac current of a line-commutated converter were described and it was shown that the trapezoidal approximation results in a more accurate model while itis still simple enough to be used in the dynamic phasor modeling.

Chapter 4

Dynamic Phasor Modeling of LCC-HVDC Systems

In this chapter a dynamic phasor-based model for a LCC-HVDC power transmission system operating under balanced operating conditions is developed. The model includes the fundamental frequency component for the ac side and the first dominant Fourier component, i.e., the zero-order term, for the dc side of the system. The developed model is then upgraded to include the first two dominant harmonics, i.e., the 11th and the 13th, on the ac side as well. This model represents the dynamics of the dc component of the dc quantities and the fundamental frequency component of the ac quantities as well as eleventh and thirteen orders harmonic.

4.1 Line Commutated Converter Model

As mentioned before in derivation of a dynamic phasor model of the LCC, a lossless converter is assumed. It is also assumed that the smoothing reactor at the dc side is adequately large so that the ripple on the dc current is negligible, i.e., $i_d \approx \langle i_d \rangle_0 = I_d$. In typical implementation two 6-pulse bridges are connected in series in what is called a 12-

pulse configuration, using Y-Y and Y-Δ transformers as shown in Figure 3-1. The 12-pulse converter arrangement offers improved harmonic spectrum (by eliminating 5^{th} and 7^{th} order harmonics of the individual 6-pulse converters) and achieves a larger dc voltage (by series connection of the two converters on the dc side).

It is instructive and convenient to firstly develop the dynamic phasor model of the 6-pulse converter. Once developed, it can be easily scaled up to the 12-pulse case. The derivation that follows pertains to the 6-pulse bridge and is directly applicable to the bottom 6-pulse converter of Figure 3-1, i.e., the converter connected to the Y-Y transformer, whose leakage inductance is shown as L_c in Figure 3-2.

The phase voltages of the ac system at the ac system side of a 6-pulse converter are as in (3-1).The $\pi/6$ phase shift of phase-a voltage is introduced merely to simplify the representation of the switching functions that are described later, and has no other bearing on the derivation.

Figure 4-1 shows the dc side voltage, as well as the voltage and current switching functions of the phase-a of the converter. A switching function serves to relate the ac- and dc-side quantities, and is obtained by inspecting the waveforms it interrelates [45]. For example, the line current i_a in Figure 3-2 can be obtained by multiplying its switching function (Figure 4-1(b)) by the dc current i_d. Note that the switching functions do include the effect of the transformer leakage inductance in creating an overlap period denoted by μ. Transitions in the current switching function are assumed to be linear as per a trapezoidal wave approximation explained in the previous chapter. It was shown in Chapter 3 that the trapezoidal approximation only has negligible impacts on the magnitude of the ac current waveform and the power factor of the converter. Nonlinear approximations for the transitions have also been proposed [9]. Switching functions for the quantities of the other phases are obtained by shifting phase-a switching functions by $2\pi/3$.

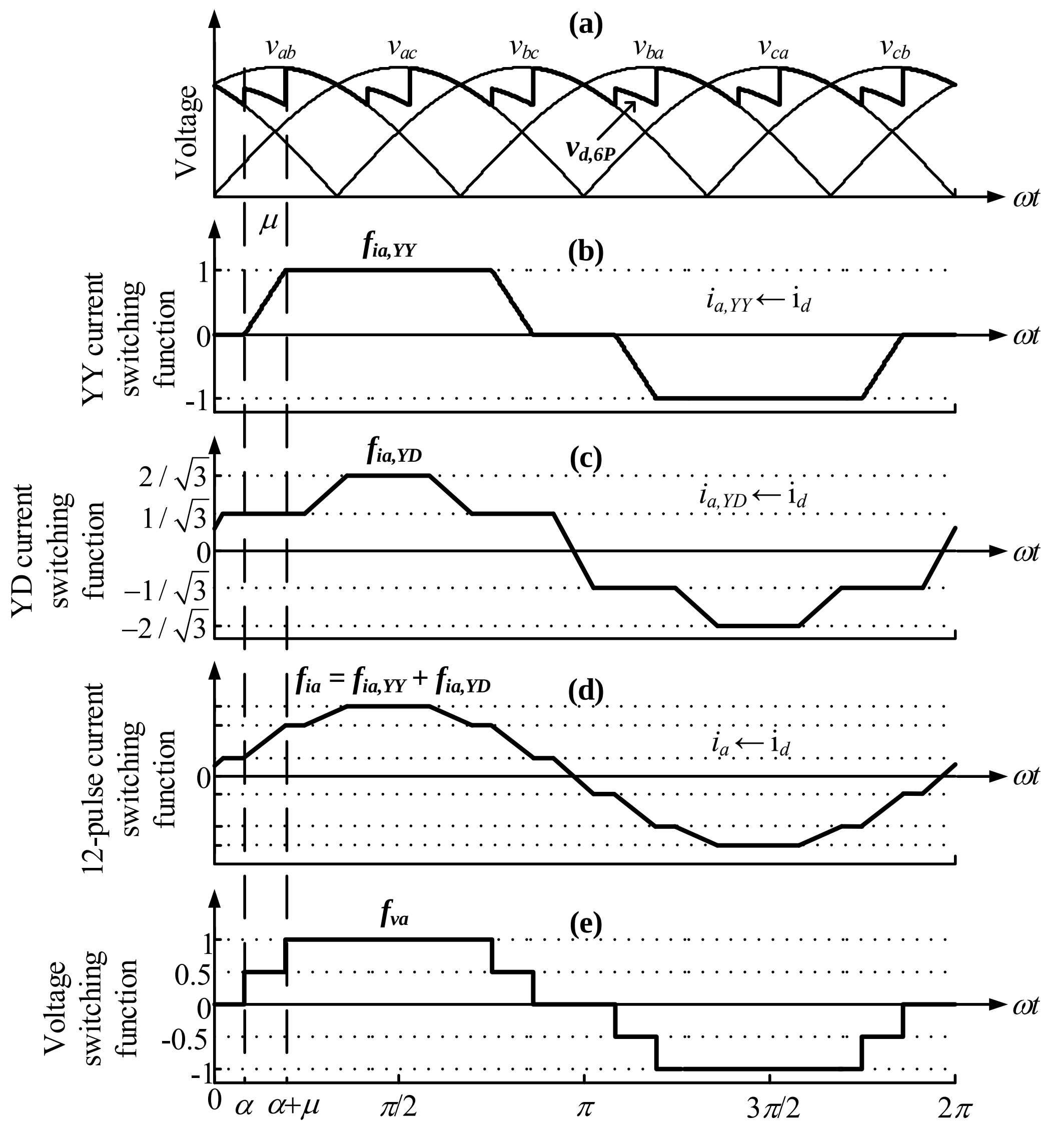

Figure 4-1: Waveforms and switching functions: (a) actual line and dc-side voltages of the 6-pulse converter; (b) current switching function for the Y-Y 6-pulse bridge; (c) current switching function for the Y-D 6-pulse bridge; (d) current switching function for the 12-pulse converter; (e) voltage switching function.

The dc-side voltage waveform of the 6-pulse converter is expressed in terms of the ac-side phase voltages and their switching functions in equation (4-1).

$$v_{d,6P} = f_{va}v_a + f_{vb}v_b + f_{vc}v_c \tag{4-1}$$

where f_{va}, f_{vb} and f_{vc} are switching functions of the voltages of phases a, b and c, respectively. The function f_{va} is given in Figure 4-1(e). The other two functions are phase-shifted versions of this switching function. To determine the dc value (0-th order component) of the dc-side voltage one can apply (2-2) with $k = 0$ to (4-1); therefore:

$$\langle v_{d,6P} \rangle_0 = \langle f_{va}v_a \rangle_0 + \langle f_{vb}v_b \rangle_0 + \langle f_{vc}v_c \rangle_0 \tag{4-2}$$

The three terms on the right-hand side of (4-2) include the averages of the products of the switching functions and phase voltages. These terms can be expanded into products of averages using (2-4), as follows.

$$\begin{aligned} \langle v_{d,6P} \rangle_0 = & \ldots + \langle f_{va} \rangle_1 \langle v_a \rangle_{-1} + \langle f_{va} \rangle_{-1} \langle v_a \rangle_1 + \ldots \\ & + \ldots + \langle f_{vb} \rangle_1 \langle v_b \rangle_{-1} + \langle f_{vb} \rangle_{-1} \langle v_b \rangle_1 + \ldots \\ & + \ldots + \langle f_{vc} \rangle_1 \langle v_c \rangle_{-1} + \langle f_{vc} \rangle_{-1} \langle v_c \rangle_1 + \ldots \end{aligned} \tag{4-3}$$

The index-1 averages of the phase-a voltage and the switching function for phase-a are obtained using (2-2) as follows. The corresponding terms for phases b and c are simply phase-shifted versions of these expressions.

$$\langle v_a \rangle_1 = \frac{V_m}{2}\cos(\frac{\pi}{6}) - j\frac{V_m}{2}\sin(\frac{\pi}{6}) \tag{4-4}$$

$$\langle f_{va} \rangle_1 = \frac{-j\sqrt{3}}{2\pi}[e^{-j(\alpha-\frac{\pi}{6})} + e^{-j(\alpha+\mu-\frac{\pi}{6})}] \tag{4-5}$$

Substituting these terms into (4-3) yields the following expression for the average dc-voltage of the 6-pulse bridge.

$$\left\langle v_{d,6P} \right\rangle_0 = V_{d,6P} = \frac{3\sqrt{3}V_m}{2\pi}[\cos\alpha + \cos(\alpha + \mu)] \\ = V_{d0,6P}\cos\alpha - R_c I_d \tag{4-6}$$

where $V_{d,6P}$ is the dc component (i.e. the average) of the dc side voltage, and

$$V_{d0,6P} = \frac{3\sqrt{3}}{\pi} V_m \tag{4-7}$$

$$R_c = \frac{3}{\pi}\omega L_c \tag{4-8}$$

The R_c is often called the *equivalent commutation resistance*, $V_{d0,6P}$ is called *ideal no-load dc voltage*, and I_d is the average of the dc current at the dc terminal of the 6-pulse converter and may vary with time [26], [46]. The amplitude of the point of common coupling (PCC) voltage (V_m) may also vary with time due to, for example, the varying amount of current through the ac line.

Similarly, it is noted that for the ac-side current the following expression holds.

$$i_{a,YY} = f_{ia,YY} i_d \tag{4-9}$$

In order to determine the fundamental-frequency component of ac current $\left\langle i_{a,YY} \right\rangle_1 = \sqrt{2} I_{YY}^{(1)} \exp(\angle I_{a,YY}^{(1)})$, (2-2) is applied to (4-9) with k = 1, which yields the expressions (4-10) and (4-11) for the magnitude and phase of the fundamental Fourier component of the phase-a current.

$$I_{YY}^{(1)} = \frac{\sqrt{6}}{\pi} I_d \frac{\sin(\frac{\mu}{2})}{(\frac{\mu}{2})} \tag{4-10}$$

$$\angle I_{a,YY}^{(1)} = \frac{\pi}{6} - \cos^{-1}\left(\frac{\cos\alpha + \cos(\alpha+\mu)}{2} \frac{(\frac{\mu}{2})}{\sin(\frac{\mu}{2})}\right) \tag{4-11}$$

Note that the $\pi/6$ term is due to the assumed phase angle of phase-a voltage (see(3-1)). In general, this must be set to the actual phase angle of the phase-a voltage.

The expressions given in (4-6), (4-10) and (4-11) describe the dynamics of the dc voltage and ac current of the 6-pulse converter. It is noted that the dc voltage of the 12-pulse converter (v_{dR} or v_{dI} in Figure 3-1) results from the series connection of two 6-pulse converters with equal average voltages. Therefore, the average of the dc voltage of the 12-pulse converter is simply obtained as follows.

$$\langle v_d \rangle_0 = V_d = 2V_{d,6P} = \frac{6\sqrt{3}}{\pi} V_m \cos\alpha - \frac{6}{\pi}\omega L_c I_d \tag{4-12}$$

where I_d is the average of the dc current of the 12-pulse converter.

Similarly, the ac-side current of the 12-pulse converter can be obtained by noting that the switching functions for ac-currents of the Y-Y and Y-Δ connected 6-pulse bridges have equal fundamental components and are in phase; i.e.,

$$\langle f_{ia,YY} \rangle_1 = \langle f_{ia,YD} \rangle_1 \tag{4-13}$$

therefore,

$$\langle i_a \rangle_1 = 2\langle i_{a,YY} \rangle_1 \tag{4-14}$$

For converter banks with higher pulse numbers, e.g., 24 or 48, it is merely enough to multiply the averaged values of the constituent 6-pulse converters by the respective number of blocks used to create the bank.

Note that the generalized averaging formula used here allows inclusion of harmonics that are ignored in conventional averaging techniques. For instance, it would have been straightforward to retain higher harmonic components if a more accurate expression for the dc-side voltage would have been desired. This flexibility in deciding the level of detail in a model is a direct benefit of the dynamic phasor modeling approach.

4.2 DC System Model

The dc system of an HVDC transmission system consists of a dc transmission line/cable and the smoothing reactors at the rectifier and inverter ends. Here a T-model is used for the dc transmission line as shown in Figure 4-2. This configuration with constant (frequency independent) lumped circuit elements is used throughout this research for all the developed models. The smoothing reactors are included in the equivalent series inductance of the line.

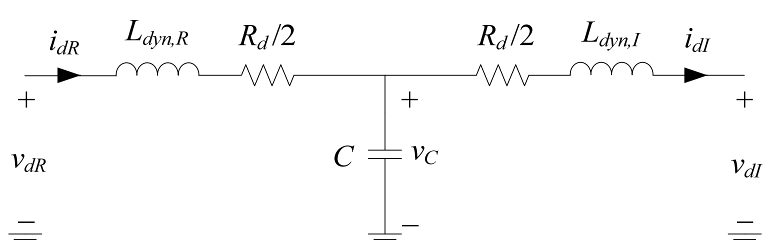

Figure 4-2: DC transmission line model.

The dynamic behaviour of the line is described using three state variables – its two inductor currents and one capacitor voltage. It can be shown that the equivalent leakage inductance of the ac transformer, seen from dc side of the converter, is different during the commutation and non-commutation periods [26]. During non-commutation intervals of a 6-pulse bridge, two ac lines each with an inductance of L_c are in series with the dc-side inductance (L_d), thereby presenting an ac equivalent inductance of $2L_c$. During the commutation period, the paralleled ac inductances of the two phases involved in commutation and the single ac-side inductance of the return path are in series, creating an ac equivalent inductance of $(3/2)L_c$. In each interval of $\pi/3$, the commutation and non-commutation periods are μ and $\pi/3-\mu$ radians long, respectively. Therefore, the average inductance of the ac system seen from the dc terminals of the 6-pulse converter will be as follows.

$$L_{c\_average} = (3/\pi)(2L_c(\frac{\pi}{3}-\mu)+\frac{3L_c}{2}\mu) = (2-\frac{3\mu}{2\pi})L_c \qquad (4\text{-}15)$$

In a converter system comprising N_B 6-pulse bridges, the average equivalent inductance of the combined ac and dc systems for each of the receiving and sending ends will therefore be as follows.

$$L_{dyn} = \frac{L_d}{2} + N_B(2-\frac{3\mu}{2\pi})L_c \qquad (4\text{-}16)$$

The L_{dyn} for the rectifier and the inverter sides may be different due to the leakage inductance of the transformer at the respective side. The dynamic equations of the dc transmission line are as follows.

$$\begin{aligned}
\frac{di_{dR}}{dt} &= \frac{1}{L_{dynR}}(v_{dR} - v_c - \frac{R_d}{2}i_{dR}) \\
\frac{di_{dI}}{dt} &= \frac{1}{L_{dynI}}(v_c - v_{dI} - \frac{R_d}{2}i_{dI}) \\
\frac{dv_c}{dt} &= \frac{1}{C}(i_{dR} - i_{dI})
\end{aligned} \qquad (4\text{-}17)$$

The dynamic phasor equivalents of these equations are obtained using (2-2) with k=0 (to denote the dc component). The resulting equations are as shown in (4-18).

$$\frac{d\langle i_{dR}\rangle_0}{dt} = \frac{1}{L_{dynR}}\left(\langle v_{dR}\rangle_0 - \langle v_c\rangle_0 - \frac{R_d}{2}\langle i_{dR}\rangle_0\right)$$
$$\frac{d\langle i_{dI}\rangle_0}{dt} = \frac{1}{L_{dynR}}\left(\langle v_c\rangle_0 - \langle v_{dI}\rangle_0 - \frac{R_d}{2}\langle i_{dI}\rangle_0\right) \qquad (4\text{-}18)$$
$$\frac{d\langle v_c\rangle_0}{dt} = \frac{1}{C}\left(\langle i_{dR}\rangle_0 - \langle i_{dI}\rangle_0\right)$$

4.3 AC Network Model

Modeling of the ac network involves development of dynamic phasor representations for components such as transformers, filters, loads, and transmission lines [9], [47]. It was shown that if the dc-side current of the converter is assumed to be purely dc, i.e., comprising only one component with a 0 Hz frequency, the fundamental component of the ac line current is a sine wave with a fixed amplitude (as shown in (4-10)) and with a frequency of f_s. During transients the dc current may undergo oscillations and hence is not constant. If the dc current, during its transient variations, has a low-frequency oscillatory component at f_o, it can be shown that the amplitude of the fundamental component of the ac line current has oscillations at f_o. This amplitude-modulated fundamental component results in two sidebands of f_s+f_o and $f_s - f_o$ [40]. If f_o is relatively small both sidebands are adequately close to f_s and the ac system may be represented using a constant admittance representation. However if f_o is large both sidebands are significantly different from f_s and the constant-admittance representation of the ac network is no longer acceptable, and dynamic phasor model of the ac network must be used to properly represent the ac network dynamics during transients [40], [48].

Consider, for example, a series RL circuit as shown in Figure 4-3. The time-domain differential equation for such a circuit is given in (4-19).

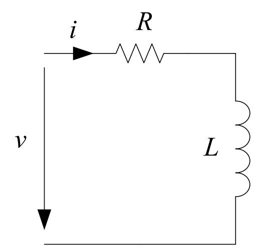

Figure 4-3: A simple RL circuit.

$$v = Ri + L\frac{di}{dt} \tag{4-19}$$

By applying (2-2) and (2-3) for k = 1 (fundamental component) to (4-19) the following dynamic phasor relationship is obtained.

$$\langle v \rangle_1 = R\langle i \rangle_1 + L(\frac{d\langle i \rangle_1}{dt} + j\omega\langle i \rangle_1) \tag{4-20}$$

where $\langle v \rangle_1$ and $\langle i \rangle_1$ are the dynamic phasors of voltage and current, respectively. Note that (4-20) reduces to the conventional phasor equivalent of the series RL circuit if the rate of change of $\langle i \rangle_1$ tends to zero. Neglecting the term $d\langle i \rangle_1/dt$ in other situations, changes the equations from differential to algebraic, albeit at the expense of reduced accuracy. Therefore, the constant-admittance matrix formulation of ac systems is in fact a special subset of the dynamic phasor model. Separating (4-20) into real and imaginary components yields the following differential equations for the circuit.

$$\begin{cases} V_R = RI_R + L\dfrac{dI_R}{dt} - \omega LI_I \\ V_I = RI_I + L\dfrac{dI_I}{dt} + \omega LI_R \end{cases} \tag{4-21}$$

where

$$\langle v \rangle_1 = V_R + jV_I, \ \langle i \rangle_1 = I_R + jI_I \tag{4-22}$$

Similar equations can be derived for RC circuits and other combinations as well. The ac system in the CIGRE HVDC model consists of an impedance for the terminating ac system and shunt-connected RLC branches for the filters and reactive components at the converter terminals [27]. Dynamic phasor models for these elements are obtained using a similar procedure and are interfaced to form a complete ac-side representation. The ac quantity dynamic phasors are complex numbers; the dc quantity dynamic phasors are real numbers. The linkage between these two sets is provided through the converter equations. Inclusion of higher order harmonics in the representation of ac quantities is simply achieved by developing dynamic equations similar to (4-20) with higher index terms, e.g., k= 11 and 13 to include 11th and 13th order harmonics of the ac-side currents.

4.4 Phase-Locked Loop (PLL) Model

A PLL is a control system for tracking the phase angle of the fundamental positive-sequence component of an ac waveform. Several PLL architectures are available; the model developed here pertains to the PLL shown in Figure 4-4 that first proposed in [49] and then further analyzed in [50]. It can, however, be readily extended to other configurations as well.

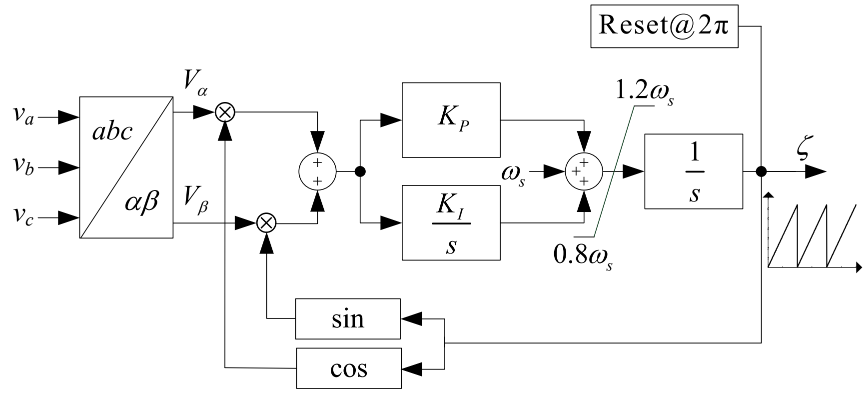

Figure 4-4: Three-phase PI-controlled phase-locked loop (PLL).

In Figure 4-4, the output ζ is a ramp train between [0,2π], which is synchronized with the positive zero-crossing of the positive-sequence fundamental component of phase-a voltage. The limits shown on the integrator input in Figure 4-4 ensure that the PLL tracks the angle of the ac waveform within a ±20% window around the nominal frequency ω_s.

From the viewpoint of the fundamental ac components, the PLL can be represented as a closed loop control system as shown in Figure 4-5. Whenever there is a change (due to perturbations in the system or changes in system set-points) in the phase angle of the voltage at the PLL point, its output undergoes a transient period before it detects and locks onto the phase angle. The closed loop system of Figure 4-5 is used to control the dynamics of this transient period.

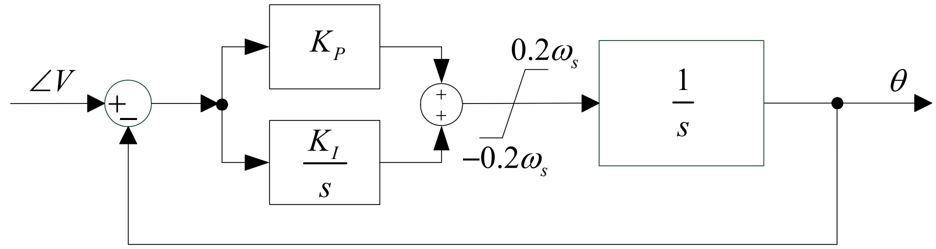

Figure 4-5: Phasor-based model of the PLL.

4.5 Inclusion of High-Order Harmonics

It is straightforward to include higher order harmonics into the model if so desired. So far the described model only includes the fundamental frequency component for the ac side and the first dominant Fourier components for the dc side of the system; i.e., the zero-order term for the dc side. Therefore, the developed model represents the dynamics of the dc component of the dc-side quantities and the fundamental frequency component of the ac-side quantities. This section aims to include the 11^{th} and 13^{th} order harmonic quantities into the ac side. It should be mentioned that addition of other harmonics is similar to adding 11^{th} and 13^{th} order harmonics.

As mentioned in Chapter 3 the case study includes a 12-pulse mono-polar HVDC transmission system, which means there is no 5^{th} or 7^{th} harmonic current injected to the ac system under idealized conditions [1]. Therefore, it was decided to include the 11^{th} and 13^{th} order harmonics into the model, which are the first dominant harmonic quantities on the ac side as an example of including higher order harmonic quantities to the system. Note that there may be small amounts of other harmonics (including 5^{th} and 7^{th}) in the ac waveform of a 12-pulse converter due to factors such as small firing angle mismatches, nonlinear distortions, or imbalances between the two converters. These harmonics are small in magnitude compared to the dominant 11^{th} and 13^{th} order harmonics of a 12-pulse converter and as such are neglected in this study. It is assumed that the current at the dc side is purely dc and the ripples on the dc current are ignored, i.e., $i_d \approx \langle i_d \rangle_0 = I_d$.

As discussed above in (4-9) the ac side current is derived by multiplying the current switching function by the dc current. The phase-a current of the Y-Y transformer is expressed as follows:

$$i_{a,YY} = f_{ia,YY} i_d \tag{4-23}$$

In order to determine the k^{th} order component of the dynamic phasor model of the current $i_{a,YY}$, (2-2) is applied to (4-23), which yields:

$$\begin{aligned} \langle i_{a,YY} \rangle_k &= \langle f_{ia,YY} i_d \rangle_k \\ &= \ldots + \langle f_{ia,YY} \rangle_{k+2} \langle i_d \rangle_{-2} + \langle f_{ia,YY} \rangle_{k+1} \langle i_d \rangle_{-1} \\ &+ \langle f_{ia,YY} \rangle_k \langle i_d \rangle_0 \\ &+ \langle f_{ia,YY} \rangle_{k-1} \langle i_d \rangle_1 + \langle f_{ia,YY} \rangle_{k-2} \langle i_d \rangle_2 + \ldots \end{aligned} \tag{4-24}$$

Based on the assumption made earlier that the dc current only contains the dc component and its ripples are ignored, $\langle i_d \rangle_k$ is zero for all values of k except when k is equal to 0. Therefore (4-24) can be simplified as follows.

$$\langle i_{a,YY} \rangle_k = \langle f_{ia,YY} \rangle_k \langle i_d \rangle_0 = I_d \langle f_{ia,YY} \rangle_k \tag{4-25}$$

After some mathematical manipulations the k^{th} order component of the phase-a current switching function of the Y-Y converter transformer, $\langle f_{ia,YY} \rangle_k$, is calculated and (4-25) can be re-written as below.

$$\langle i_{a,YY} \rangle_k = \frac{2}{3} I_d \operatorname{sinc}\left(k\frac{\pi}{3}\right) \operatorname{sinc}\left(k\frac{\mu}{2}\right) e^{-ik\left(\frac{\pi}{2} - \angle V + \cos^{-1}\left(\frac{\cos\alpha + \cos(\alpha+\mu)}{2\operatorname{sinc}\left(\frac{\mu}{2}\right)}\right)\right)} \tag{4-26}$$

where sinc(x)=sin(x)/x and $\angle V$ is the phase angle of phase-a of the commutating voltage. A similar procedure is followed to derive k^{th} order components of phase-a of the ac current for the Y-Δ converter transformer $\langle f_{ia,Y\Delta}\rangle_k$. The k^{th} order components of phase-a of the ac current injected to the ac system can then easily be calculated by adding $\langle f_{ia,Y\Delta}\rangle_k$ and $\langle f_{ia,YY}\rangle_k$.

After developing the formula of the injected ac current to the ac network for any specific harmonic order, the dynamic phasor model of the ac network for any desired harmonic order needs to be determined. The dynamic phasor model of the ac network for the fundamental frequency component is shown in Chapter 3. The following extends the discussed concept to include other harmonic components into the ac network.

The same RL circuit shown in Figure 4-3 is considered here in this section as an example. By applying (2-2) and (2-3) to the time domain differential equation of the RL circuit (4-19), dynamic phasor relationship of the RL network is obtained as follows.

$$\langle v\rangle_k = R\langle i\rangle_k + L\Big(\frac{d\langle i\rangle_k}{dt} + j\omega\langle i\rangle_k\Big) \tag{4-27}$$

where $\langle v\rangle_k$ and $\langle i\rangle_k$ are the k^{th} order dynamic phasors of the voltage and current, respectively. Separating (4-27) into real and imaginary components yields the following differential equations for the circuit.

$$\begin{cases} \langle v\rangle_{k,R} = R\langle i\rangle_{k,R} + L\dfrac{d\langle i\rangle_{k,R}}{dt} - L\omega\langle i\rangle_{k,I} \\ \langle v\rangle_{k,I} = R\langle i\rangle_{k,I} + L\dfrac{d\langle i\rangle_{k,I}}{dt} + L\omega\langle i\rangle_{k,R} \end{cases} \tag{4-28}$$

where

$$\langle v\rangle_k = \langle v\rangle_{k,R} + j\langle v\rangle_{k,I}\,,\ \langle v\rangle_k = \langle v\rangle_{k,R} + j\langle v\rangle_{k,I} \tag{4-29}$$

A similar method is used for other network configurations (like an RC circuit) to develop the dynamic phasor models associated with the network for selected harmonic orders.

4.6 Model Validation and Results

A dynamic phasor-based model for the CIGRE HVDC benchmark model [27] is developed in MATLAB/SIMULINK as per the procedures in this chapter. The benchmark model has a power circuitry and control layout similar to Figure 3-1 and Figure 3-8.

The developed dynamic phasor model is validated against a detailed switching model that is implemented in the PSCAD/EMTDC electromagnetic transient simulator. While this involves validation of a computer simulation model against another computer simulation model, it must be noted that electromagnetic transient simulations (conducted using small enough time steps on commercial grade simulators) are widely regraded as highly accurate representations of the actual behavior of power systems [51], [52], [53], [54]. Therefore, use of EMT simulation results as a benchmark for validation of other simulation methods is a common practice in power systems [4], [26], [41].

In order to ensure that the benchmark EMT results (using an EMT simulation tool) are indeed accurate, one must use small enough simulation time-steps. Analytical determination of a small enough time-step is often not possible, due to the nonlinear and complicated nature of systems under consideration. The practice of choice is to use trial and error using successively decreasing time-steps and to observe the results. The time-step below which no notable change in the generated results is observed is adopted. In the simulation cases that are presented next, a time-step of 20 μs is used in all PSCAD/EMTDC simulations.

In order to investigate the accuracy of the dynamic phasor model in representing transients below the switching frequency, a third model of the system is also used, in which the bridge converters are modeled as an averaged model; however, the ac system is represented using a constant admittance-matrix. In this model the passive elements of the ac systems at the rectifier and the inverter sides are represented using impedances at the fundamental frequency of 50 Hz. This constant-admittance matrix model ignores the time variations of the Fourier components of the line current. Note that the constant-admittance matrix model is a simplification of the dynamic phasor model in which the time-derivatives of the Fourier coefficients are set to zero as was discussed in Section 4.3.

Four case studies involving all three models are presented:

Case 1: Rectifier side dynamics;

Case 2: Complete system dynamics;

Case 3: Fault analysis with and without commutation failure;

Case 4: High-order harmonics;

A simulation time-step of 1000 μs is used in the simulation of the low-frequency dynamics using the dynamic phasor model (cases 1 to 3). For the simulations in case 4, wherein harmonics are also included, a time-step of 100 μs is used for the dynamic phasor model. Similar to an EMT solver, use of excessively large time-steps in a dynamic phasor solver will adversely impact the accuracy of its results. The simulation time-steps reported for the developed dynamic phasor model are selected using trial and error in a manner similar to the selection of time-steps for an EMT solver.

The system specifications for both power circuitry and control layout used in the case studies are mentioned in Table 4-1 and Table 4-2.

Table 4-1: CIGRE HVDC Benchmark System Data

Parameter	Rectifier	Inverter
AC voltage base values	345 kV	230 kV
Base MVA	1000 MVA	1000 MVA
Nominal dc voltage	500 kV	500 kV
Nominal dc current	2 kA	2 kA
Rated trans. voltages	345:211.42 kV	211.42:230 kV
Transformers leakage	0.18 pu	0.18 pu
Filter VAR supply	625 MVAR	625 MVAR
Nominal angle	α = 15°	γ= 15°

Table 4-2: Controller Parameters for the Case Study

Controller	Parameter	Rectifier	Inverter
Phase-locked loop	Proportional gain	10	10
	Integral gain	50	50
Current controller	Proportional gain	0.1	0.63
	Integral gain	100	65.617
Gamma controller	Min. commutation margin	-	15°
	Max. margin error	-	30°
	Proportional gain	-	0.5
	Integral gain	-	20

4.6.1 Case 1: Rectifier side dynamics

For the simulation of Case 1, the inverter side is modeled as a constant dc source of 500 kV (replacing v_c in Figure 4-2). The rectifier control system follows its dc-current order via adjusting the converter's firing angle. A PLL locked onto the rectifier PCC maintains synchronism with the ac voltage and provides a reference for generation of the firing pulses.

Figure 4-6 shows the response of the system to a step change in the current order from 1.1 to 0.9 pu. Three traces generated by the three models are shown. The dynamic phasor model follows the transient simulation model's response excluding the high-frequency switching contents. The constant admittance matrix model fails to show the transient oscillations of the actual response, although it settles into the correct steady state value. As shown in Figure 4-6, the system response has damped oscillations at a frequency of approximately 62 Hz. The dynamic phasor model successfully predicts these oscillations. These oscillations are, however, far too rapid for the constant admittance-matrix representation, and hence are absent in its predicted response. It must be noted that the 62-Hz oscillations occur in the first dominant Fourier component of the dc current, i.e., the 0-order term, for which a dynamic phasor model is developed. Prediction of these oscillations does not require inclusion of additional Fourier components as the harmonic contents of the dc current of a 12-pulse converter (with symmetrical firing) includes the considered dc component as well as $12n$ harmonics (720 Hz, 1440 Hz, etc.), which are by far higher than 62 Hz.

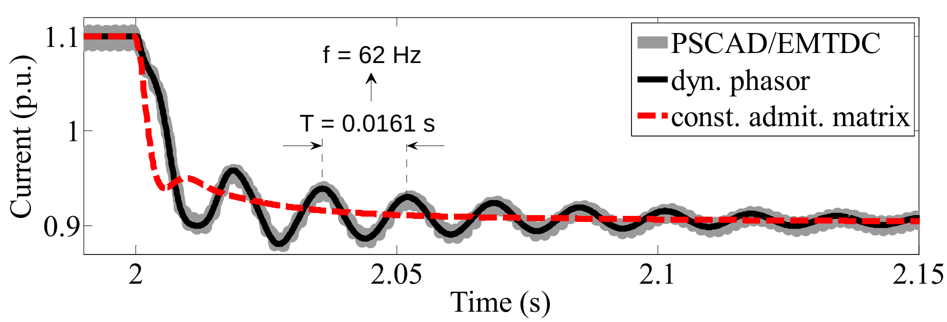

Figure 4-6: Step response of the dc current.

4.6.2 Case 2: Complete system dynamics

The complete system model with both converters and their respective ac systems and with a current controller on the rectifier side and constant extinction-angle controller on the inverter side with a VDCOL is considered. Figure 4-7 shows the step response of the system to a large current-order change from 1.05 to 0.5 pu. The rectifier current controller is engaged to adjust its firing angle. The inverter controller maintains its extinction angle at 15°. The figure also shows the dynamics of the ac voltage magnitude at the rectifier PCC.

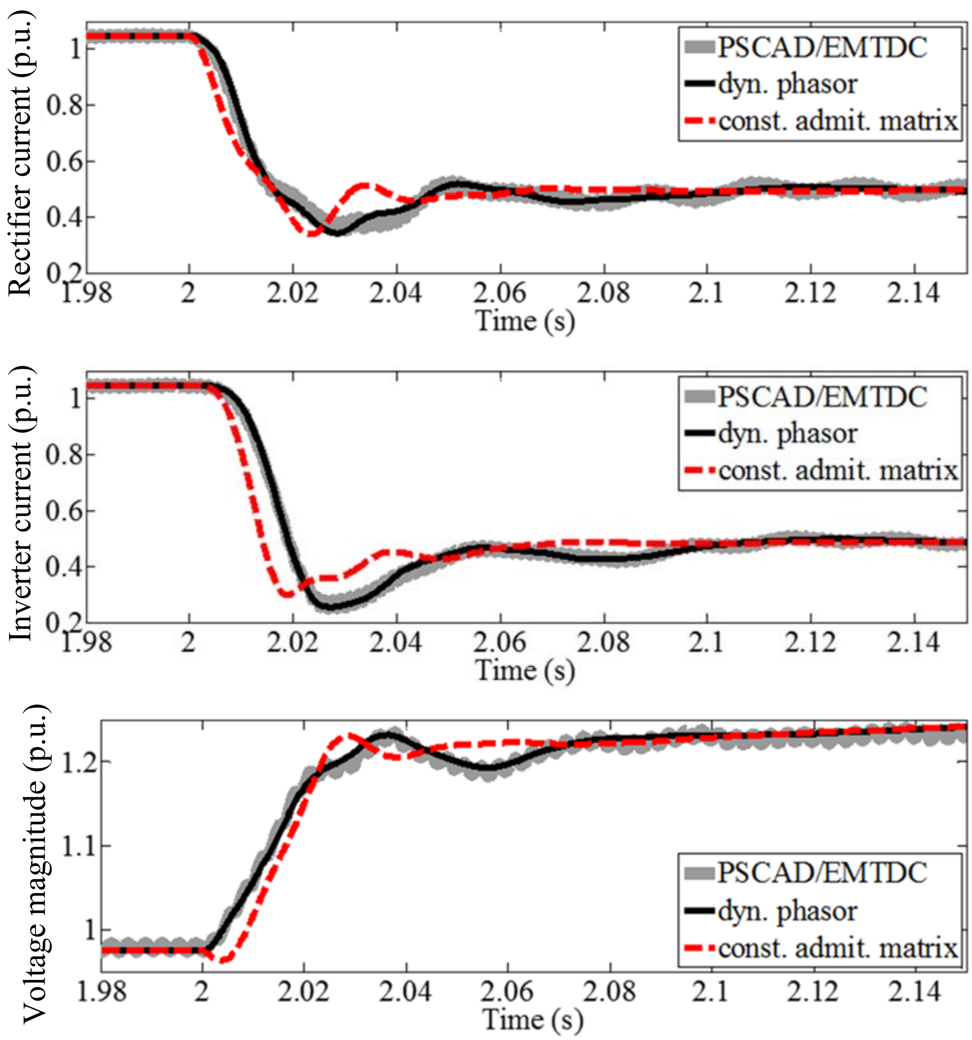

Figure 4-7: Response of the system to a step change in the current order. top: rectifier current, middle: inverter current, bottom: PCC ac voltage

The dynamic phasor model follows the system response including the sharp rise of the voltage at the inception of the step change at t = 2.0 s. The traces in Figure 4-7 show conformity between the EMT and the dynamic phasor models of the system, except for the high-frequency ripple, which is ignored in the averaging process. The constant-admittance matrix model does not accurately follow the transients, as it shows an earlier peak voltage, a smaller magnitude of oscillations, and a quicker settlement into steady state.

4.6.3 Case 3: Fault analysis with and without commutation failure

Performance of the models in representing faults is assessed in two stages. In the first stage, adequately remote faults, which do not result in commutation failures, are considered. Figure 4-8 and Figure 4-9 show the rectifier and inverter current waveforms when the magnitude and phase angle of the inverter-side ac voltage are changed by 5% and 10°, respectively. Such changes may occur due to remote faults and while they disturb the operation of the system, they are not severe enough to lead to commutation failure. As shown, both the EMT and the dynamic phasor models correctly represent the dynamics of the response. The constant-admittance matrix model, however, has considerable error during the transient period, as it predicts a larger peak at an earlier time, and settles into steady state faster. These indicate inaccuracies in both the magnitude and damping of oscillatory modes.

The faults are modeled using changing the voltage of the equivalent ac networks at the rectifier and inverter sides. It is, however, possible to apply faults at any location using an impedance to ground at that location.

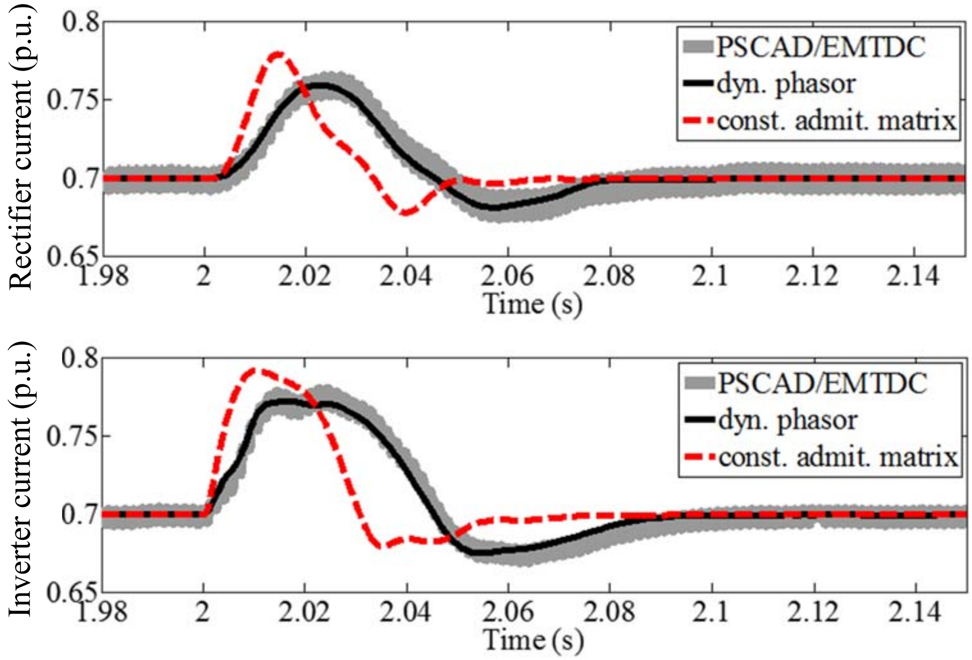

Figure 4-8: Response of the system to a 5% reduction in the inverter-side ac voltage magnitude. top: rectifier current, bottom: inverter current.

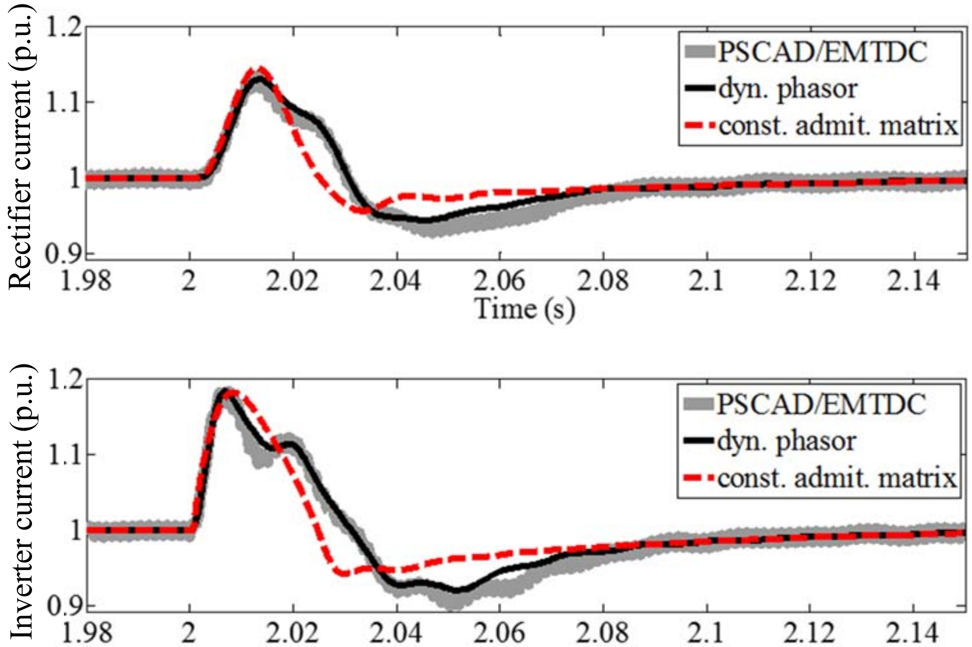

Figure 4-9: Response of the system to a -10° change in the inverter-side ac voltage phase angle. top: rectifier current, bottom: inverter current.

Figure 4-10 shows the response of the model to a severe fault in the inverter-side ac system. The fault is modeled with a 20% reduction in the ac voltage magnitude. The EMT model clearly indicates commutation failure. Both the dynamic phasor and the constant-admittance matrix models have large error during the transient period, although they converge to the correct steady state value. The reason for the discrepancy in the transient period is that these two models are developed without provisions for operation of the converter under abnormal conditions, which occur during commutation failure.

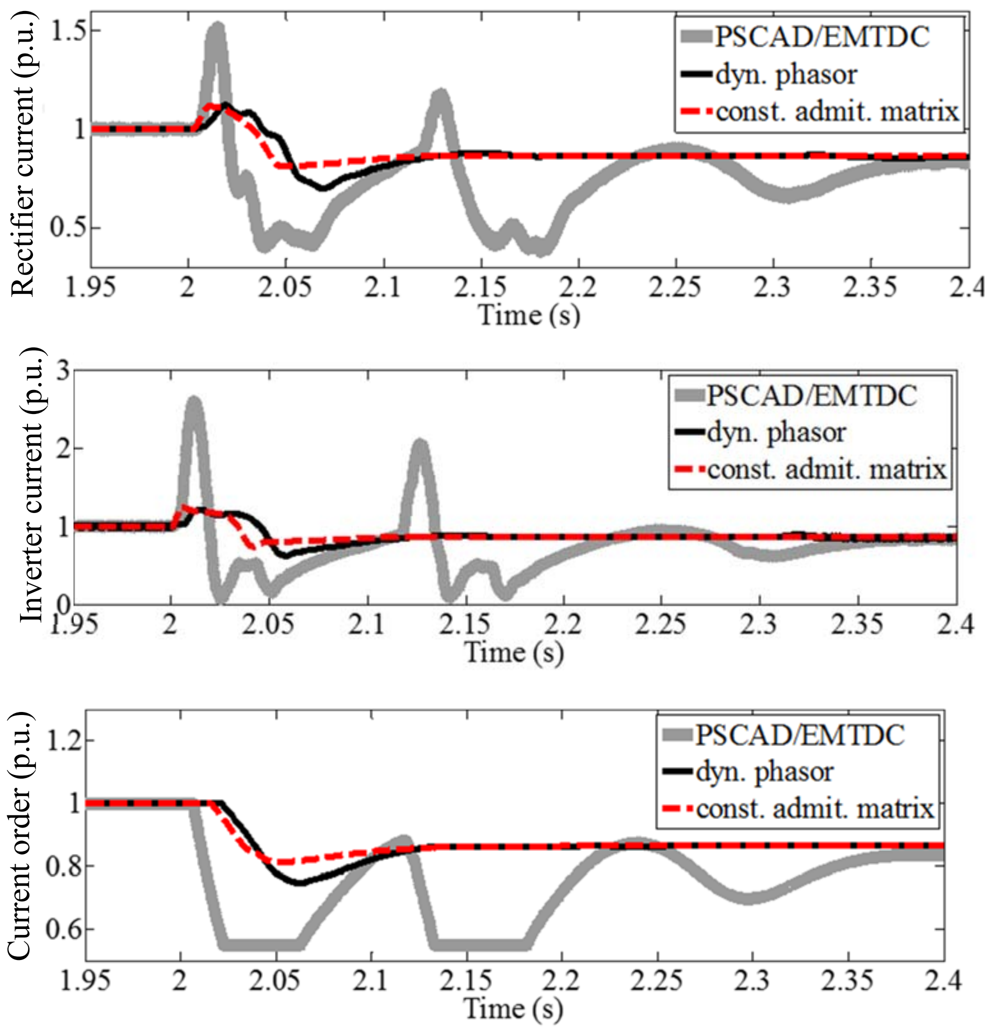

Figure 4-10: Response of the system to a 20% reduction in the inverter-side ac voltage magnitude top: rectifier current, middle: inverter current, bottom: current order.

4.6.4 High-order harmonics

All the cases so far have used only the fundamental frequency components. It was, however, previously discussed that it is possible to add any number of high-order harmonics is so desired. Figure 4-11 shows the current at one of the ac filter branches with and without considering the 11th and 13th order components of the dynamic phasor simulation. In this case, a step change is applied to the dc current order of the rectifier from 1 to 0.8 pu while the inverter is modeled as a constant dc source of 500 kV.

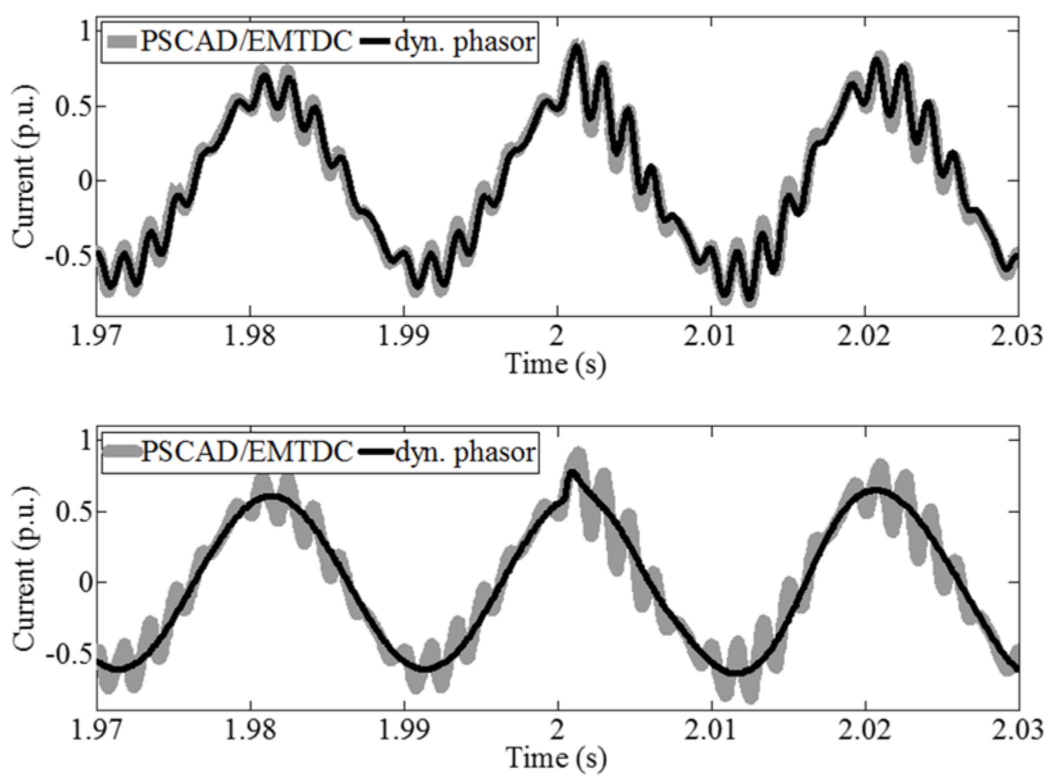

Figure 4-11: Current at one of the ac filter branches with (top) and without (bottom) considering the 11th and 13th order components of the dynamic phasor simulation.

4.7 Discussions

It is necessary to investigate the benefits of modeling using dynamic phasors in accelerating the simulation. EMT simulations normally require a small time-step in the order of 5-50 μs, to correctly predict the high-frequency switching transients. Since these high-frequency components are neglected in dynamic phasor modeling, it is expected that larger time steps can be used, which lead to speed-ups in the simulation time. The simulations shown in this case study are conducted with a time step of 20 μs for the EMT model and 1000 μs for the dynamic phasor and the constant admittance-matrix models. Since the EMT model and the two average models are not implemented in the same simulation platform, it is not directly possible to compare their simulation speed. It is, however, expected that the reduced computational intensity of the average models, due to their much larger time step, will considerably reduce their simulation time.

It should be mentioned that one might argue that acceleration of EMT simulation can be achieved by using larger time steps. While this may be achievable to some extent for a small range of time steps, it cannot be extended to large time steps. EMT models include a high level of detail and a large time step might jeopardize the ability to capture them. For example, switching commands to valves are issued at a fine rate and use of a large time step may result in missed firing pulse and hence mal-representation of the converter operation, and subsequently incorrect results for the rest of the system. At adequately large time steps, EMT simulation solvers may also experience divergence. As an example, the following figure shows the response of the dc current on the rectifier side using EMT simulations with time steps of 20 and 500 μs. The traces clearly show the deterioration of the accuracy when the time step is increased to 500 μs. As seen the trace obtained with a large time step of 500 μs clearly predicts much lower peaks an at earlier instants of time during the transient oscillations.

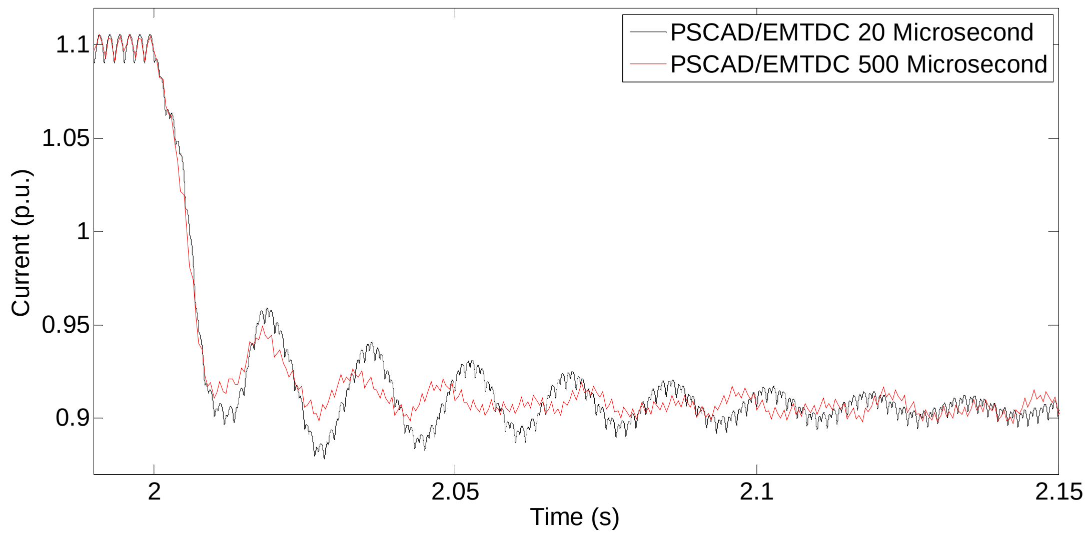

Figure 4-12: The response of the dc current on the rectifier side using EMT simulations with time steps of 20 μs and 500 μs.

4.8 Chapter Summary

In this chapter the dynamic phasor model of a LCC-HVDC transmission system operating under balanced and normal (no commutation failures) conditions were developed. The chapter described how to derive the dynamic phasor models of various parts of a LCC-HVDC transmission system including line-commutated converter, DC system, AC network, and phase-locked loop.

The model was first developed only for the fundamental frequency components (50 Hz) at the ac side quantities. However, it was shown how straightforward it is to include higher harmonic orders if so desired. As an example the 11th and 13th order harmonic components were added to the developed model. Various simulations were performed to validate the accuracy of the developed models.

Chapter 5

Unbalanced Conditions and Commutation Failure

In the previous chapter the dynamic phasor model of a LCC-HVDC was developed. However, the developed model had a number of limitations as it worked properly only for balanced and normal (i.e., no commutation failure) operating conditions. Therefore, this model is not able to fully model the transient phenomena that may occur in an HVDC system.

This chapter extends the model in order to properly represent a LCC-HVDC system operating under unbalanced conditions and during commutation failure. Unbalanced conditions may arise as a result of unbalanced faults, such as a single line to ground fault, at the ac side of the converter; severe faults can cause commutation failure in the converter system in particular at the inverter.

5.1 Modeling for Unbalanced Conditions

In this section the developed model in Chapter 4 is modified in order to derive the dynamic phasor model of a line-commutated converter operating under unbalanced conditions. Developing a dynamic phasor model of LCC to properly work under unbalanced conditions can be of great help to investigate the behaviour of the system during unbalanced faults such as single-phase to ground faults, double-phase faults, and double-phase to ground faults. This is advantageous as there has not been substantial work to analytically investigate operating characteristics of LCC-HVDC transmission systems during unbalanced voltage conditions.

The term “unbalanced operating conditions” in this chapter is applied to situations where the LCC AC voltages are not balanced due to any reason. In other words, there are other types of unbalanced operating conditions that are NOT considered in this thesis (e.g., different impedance values for three phases or different loading for different phases). It is, however, possible to extend the model to include other types of unbalanced operating conditions as well.

In this section firstly the dynamic phasor model of a line-commutated converter operating under unbalanced condition will be developed. The developed model can then be used to derive the ac current at the ac side of the YY converter transformer. This is because the current at the two sides of a YY transformer have similar waveforms.

The developed model will then be modified and expanded in order to be able to properly simulate a LCC connected to a YD transformer operating under unbalanced conditions.

The above mentioned two models will then be combined to fully model a 12-pulse bridge.

5.1.1 Line-commutated converter under unbalanced conditions

In this section the dynamic phasor model of a line-commutated converter operating under unbalanced conditions is developed. For convenience the schematic diagram of a LCC is shown again in Figure 5-1.

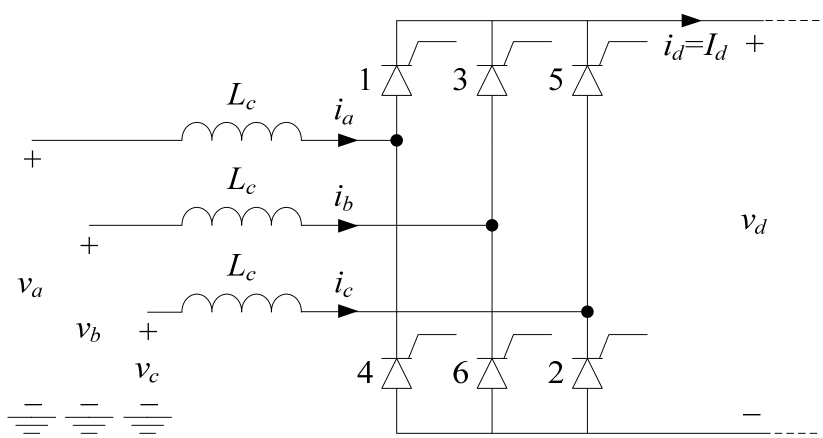

Figure 5-1: Circuit diagram of a line commutated converter (LCC)

It is assumed that ac voltages have some negative-sequence contents (unbalanced operating conditions) and as such the instantaneous voltages are as follows.

$$\begin{cases} v_a = V_P \sin(\omega t + \varphi_{aP}) + V_N \sin(\omega t + \varphi_{aN}) \\ v_b = V_P \sin\left(\omega t + \varphi_{aP} - \dfrac{2\pi}{3}\right) + V_N \sin\left(\omega t + \varphi_{aN} + \dfrac{2\pi}{3}\right) \\ v_c = V_P \sin\left(\omega t + \varphi_{aP} + \dfrac{2\pi}{3}\right) + V_N \sin\left(\omega t + \varphi_{aN} - \dfrac{2\pi}{3}\right) \end{cases} \tag{5-1}$$

where

V_P : voltage magnitude of the positive sequence component

φ_{aP} : phase angle of phase-a for the positive sequence component

V_N : voltage magnitude of the negative sequence component

φ_{aN} : phase angle of phase-a for the negative sequence component

The line voltage can be calculated using (5-1) as follows.

$$\begin{cases} v_{ab} = \sqrt{3}V_P \sin\left(\omega t + \varphi_{aP} + \frac{\pi}{6}\right) + \sqrt{3}V_N \sin\left(\omega t + \varphi_{aN} - \frac{\pi}{6}\right) \\ v_{bc} = \sqrt{3}V_P \sin\left(\omega t + \varphi_{aP} - \frac{\pi}{2}\right) + \sqrt{3}V_N \sin\left(\omega t + \varphi_{aN} + \frac{\pi}{2}\right) \\ v_{ca} = \sqrt{3}V_P \sin\left(\omega t + \varphi_{aP} + \frac{5\pi}{6}\right) + \sqrt{3}V_N \sin\left(\omega t + \varphi_{aN} - \frac{5\pi}{6}\right) \end{cases} \tag{5-2}$$

To make the analysis simple the ratio of imbalance is defined as the voltage magnitude of the negative sequence component divided by the voltage magnitude of the positive sequence component. In addition to that the angle φ is defined as the angle difference between the negative and the positive sequence components of phase-a voltage. These are shown as follows.

$$K = \frac{V_N}{V_P} \tag{5-3}$$

$$\varphi = \varphi_{aN} - \varphi_{aP} \tag{5-4}$$

In order for a thyristor to be turned ON the voltage across its anode-cathode terminals needs to be positive when the firing pulses are applied to its gate terminal. Therefore, it is possible that the valve cannot be turned ON when firing pulses are applied as the voltage across its anode-cathode terminals is not positive yet. This phenomenon can happen under unbalanced operating conditions for which the firing angle is calculated and applied based on the ac voltage angle measured by a PLL; as it was mentioned earlier a PLL is a control system for tracking the phase angle of the fundamental <u>positive-sequence</u> component of an ac waveform.

The firing pulses in LCC-HVDC systems are calculated based on fundamental positive-sequence components of phase-a and are applied to valve 1 and then to valve 2 for which the phase angle calculated for valve 1 is shifted $\pi/6$. The same equidistant pattern of shifting by $\pi/6$ is continued for other valves as well.

For the reason discussed above for a LCC operating under unbalanced conditions there is a minimum firing angle required for each phase in order to turn ON the valves of that phase once the firing pulses are applied. The minimum firing angle for each valve is calculated such that the voltage across the anode-cathode terminal for that valve becomes positive. The minimum firing angle required for each phase is as follows.

$$
\alpha_{a,\min} = \tan^{-1}\left(\frac{\sin\left(\varphi_{aP} + \frac{5\pi}{6}\right) + K\sin\left(\varphi_{aN} - \frac{5\pi}{6}\right)}{-\cos\left(\varphi_{aP} + \frac{5\pi}{6}\right) - K\cos\left(\varphi_{aN} - \frac{5\pi}{6}\right)} \right)
$$

$$
\alpha_{b,\min} = \tan^{-1}\left(\frac{-\sin\left(\varphi_{aP} - \frac{\pi}{6}\right) - K\sin\left(\varphi_{aN} + \frac{5\pi}{6}\right)}{\cos\left(\varphi_{aP} - \frac{\pi}{6}\right) + K\cos\left(\varphi_{aN} + \frac{5\pi}{6}\right)} \right) \tag{5-5}
$$

$$
\alpha_{c,\min} = \tan^{-1}\left(\frac{\sin\left(\varphi_{aP} + \frac{5\pi}{6}\right) + K\sin\left(\varphi_{aN} + \frac{\pi}{2}\right)}{-\cos\left(\varphi_{aP} + \frac{5\pi}{6}\right) - K\cos\left(\varphi_{aN} + \frac{\pi}{2}\right)} \right)
$$

If the firing angle is less than the minimum firing angle for that phase, the minimum firing angle will be used for that phase in the dynamic phasor equations. As previously discussed this phenomenon is what actually happens in real HVDC systems due to the tracking of the fundamental positive-sequence phase by a PLL.

5.1.2 Commutation period

In order to develop the dynamic phasor-based model of a LCC operating under unbalanced conditioned the current and voltage switching functions need to be re-defined. Calculation of commutation periods is the first step to develop the current and voltage switching functions. Therefore, in this section the commutation period of a LCC operating under unbalanced conditions is derived.

The procedure is similar to the calculations of commutation period of LCC operating under balanced conditions. To find the commutation period between valves 1 and 5, when the dc voltage transfers from v_{cb} to v_{ab} as shown in Figure 3-4, the set of equations in (5-6) must be solved.

$$\begin{cases} v_a - L_s \dfrac{di_a}{dt} = v_c - L_s \dfrac{di_c}{dt} \\ i_c = I_d - i_a \\ i_a(\omega t = \alpha) = 0 \\ i_a(\omega t = \alpha + \mu) = I_d \end{cases} \tag{5-6}$$

As mentioned before if in the above equations the firing angle (α) is less than the minimum firing angle ($\alpha_{a,min}$ in (5-5)) then the firing angle will be replaced with the minimum firing angle.

Solution of the equation in (5-6) results in the following expression for μ_a.

$$\begin{aligned} \mu_a = {} & \sin^{-1}\left(\frac{A + K\cos\left(\alpha + \varphi - \frac{2\pi}{3}\right) - \cos(\alpha)}{\sqrt{\left(K\sin\left(\varphi - \frac{2\pi}{3}\right)\right)^2 + \left(K\cos\left(\varphi - \frac{2\pi}{3}\right) - 1\right)^2}} \right) \\ & - \tan^{-1}\left(\frac{K\cos\left(\varphi - \frac{2\pi}{3}\right) - 1}{-K\sin\left(\varphi - \frac{2\pi}{3}\right)} \right) - \alpha \end{aligned} \tag{5-7}$$

where

$$A = \frac{2\omega L_c I_d}{\sqrt{3} V_P} \tag{5-8}$$

A similar procedure is followed for phases b and c to derive the commutation period formulas for other phase. (5-9) and (5-10) show the commutation period for phases b and c for a LCC operating under unbalanced conditions.

$$\mu_b = \sin^{-1}\left(\frac{A + K\cos\left(\alpha + \varphi + \frac{2\pi}{3}\right) - \cos(\alpha)}{\sqrt{\left(K\sin\left(\varphi + \frac{2\pi}{3}\right)\right)^2 + \left(K\cos\left(\varphi + \frac{2\pi}{3}\right) - 1\right)^2}}\right) - \tan^{-1}\left(\frac{K\cos\left(\varphi + \frac{2\pi}{3}\right) - 1}{-K\sin\left(\varphi + \frac{2\pi}{3}\right)}\right) - \alpha \tag{5-9}$$

$$\mu_c = \sin^{-1}\left(\frac{A + K\cos(\alpha + \varphi) - \cos(\alpha)}{\sqrt{(K\sin(\varphi))^2 + (K\cos(\varphi) - 1)^2}}\right) - \tan^{-1}\left(\frac{K\cos(\varphi) - 1}{-K\sin(\varphi)}\right) - \alpha \tag{5-10}$$

5.1.3 DC voltage switching functions

In this section the dynamic phasor equations of the dc voltage of a LCC operating under unbalanced conditions are derived. As explained in Chapter 4 the dc side voltage waveform of the 6-pulse converter can be expressed in terms of the ac-side phase voltages and their switching functions as follows.

$$v_d = f_{vaU}\, v_a + f_{vbU}\, v_b + f_{vcU}\, v_c \tag{5-11}$$

where f_{vaU}, f_{vbU} and f_{vcU} are the voltage switching functions of a LCC operating under unbalanced conditions for phases a, b, and c, respectively. The functions f_{vaU}, f_{vbU} and f_{vcU} are shown in Figure 5-2.

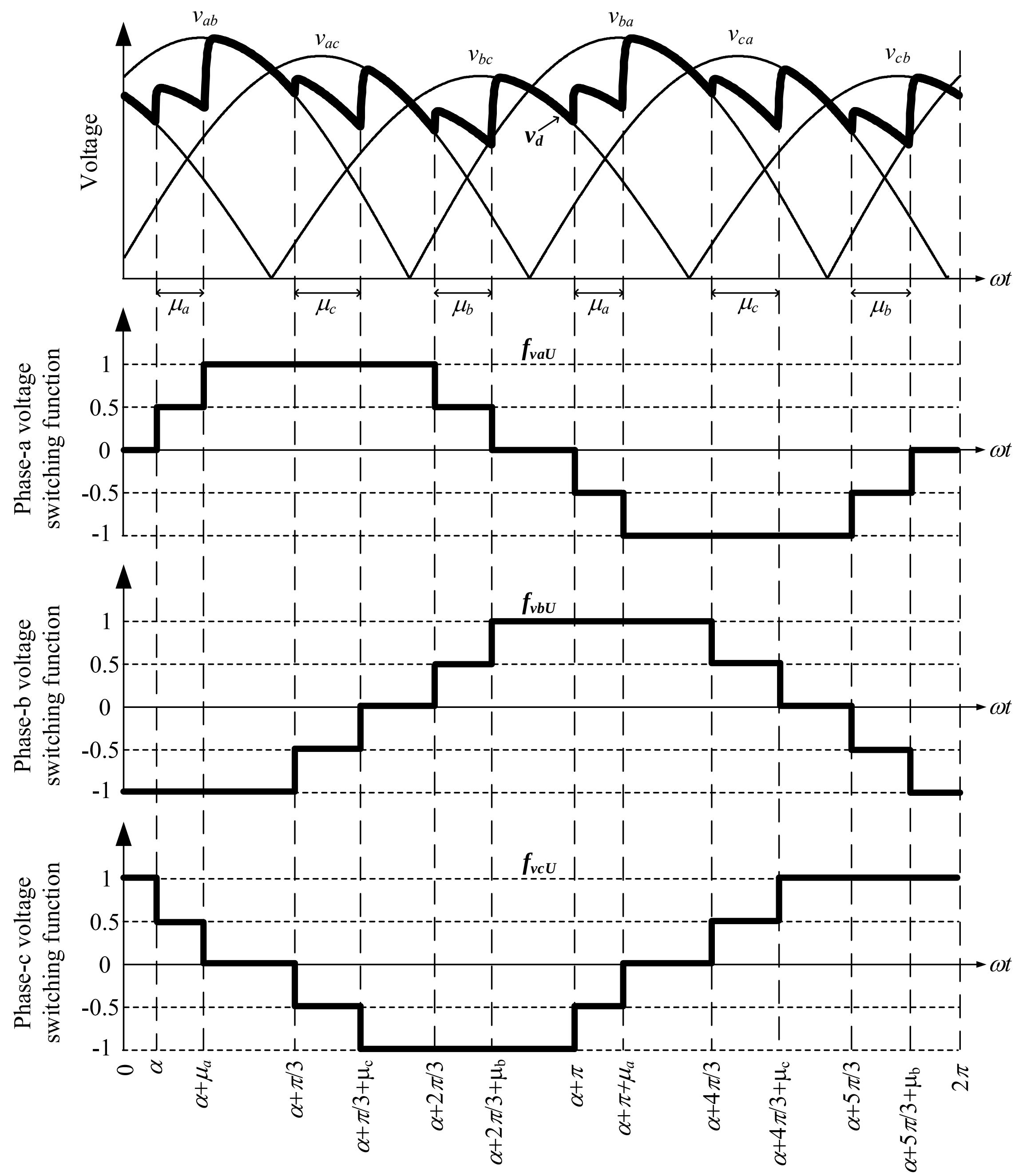

Figure 5-2: Voltage switching functions of phases a, b, and c for unbalanced condition. The DC side voltage of the LCC is also showed at the top waveform.

It is known that in the presence of unbalanced ac voltages in a LCC the dc voltage of the converter will have a second harmonic component in addition to the dc component.

Therefore, to develop the dynamic phasor equations of the dc voltage for a LCC operating under unbalanced conditions both the zero- and second-order components of (2-2) are considered.

To determine the dc value (0-th order component) of the dc-side voltage one can apply (2-2) with $k = 0$ to (5-11); therefore:

$$\langle v_d \rangle_0 = \langle f_{vaU}\, v_a \rangle_0 + \langle f_{vbU}\, v_b \rangle_0 + \langle f_{vcU}\, v_c \rangle_0 \tag{5-12}$$

The three terms on the right-hand side of (5-12) include the averages of the products of the switching functions and phase voltages. These terms can be expanded into products of averages using (2-4), as follows.

$$\begin{aligned} \langle v_d \rangle_0 = \ldots &+ \langle f_{vaU} \rangle_1 \langle v_a \rangle_{-1} + \langle f_{vaU} \rangle_{-1} \langle v_a \rangle_1 + \ldots \\ + \ldots &+ \langle f_{vbU} \rangle_1 \langle v_b \rangle_{-1} + \langle f_{vbU} \rangle_{-1} \langle v_b \rangle_1 + \ldots \\ + \ldots &+ \langle f_{vcU} \rangle_1 \langle v_c \rangle_{-1} + \langle f_{vcU} \rangle_{-1} \langle v_c \rangle_1 + \ldots \end{aligned} \tag{5-13}$$

A similar procedure is taken to derive the second component of the dc voltage. To determine the dc second order component of the dc-side voltage one can apply (2-2) with $k = 2$ to (5-11); therefore:

$$\langle v_d \rangle_2 = \langle f_{vaU}\, v_a \rangle_2 + \langle f_{vbU}\, v_b \rangle_2 + \langle f_{vcU}\, v_c \rangle_2 \tag{5-14}$$

The three terms on the right-hand side of (5-14) can be expanded using (2-4), as follows.

$$\begin{aligned} \langle v_d \rangle_2 = \ldots &+ \langle f_{vaU} \rangle_1 \langle v_a \rangle_1 + \langle f_{vaU} \rangle_3 \langle v_a \rangle_{-1} + \ldots \\ + \ldots &+ \langle f_{vbU} \rangle_1 \langle v_b \rangle_1 + \langle f_{vbU} \rangle_3 \langle v_b \rangle_{-1} + \ldots \\ + \ldots &+ \langle f_{vcU} \rangle_1 \langle v_c \rangle_1 + \langle f_{vcU} \rangle_3 \langle v_c \rangle_{-1} + \ldots \end{aligned} \tag{5-15}$$

It should be mentioned that the dynamic phasor equations of ac voltages only include 1 and -1 components (i.e., $\langle v_a \rangle_1$ and $\langle v_a \rangle_{-1}$) and all the other components are equal to zero.

Therefore, the results of their products to other terms are zero. The k^{th} factors of voltage switching functions are as follows.

$$\langle f_{vaU}\rangle_k = \frac{j}{4\pi k}\left[-1-e^{-jk\mu_a}+e^{-jk\frac{2\pi}{3}}+e^{-jk(\mu_b+\frac{2\pi}{3})}\right]\left(1-e^{-jk\pi}\right)e^{-jk\left(\alpha+\frac{\pi}{6}-\varphi_{aP}\right)}$$

$$\langle f_{vbU}\rangle_k = \frac{j}{4\pi k}\left[-1-e^{-jk\mu_b}+e^{-jk\frac{2\pi}{3}}+e^{-jk(\mu_c+\frac{2\pi}{3})}\right]\left(1-e^{-jk\pi}\right)e^{-jk\left(\alpha+\frac{\pi}{6}-\varphi_{aP}\right)}e^{-jk\frac{2\pi}{3}} \quad (5\text{-}16)$$

$$\langle f_{vcU}\rangle_k = \frac{j}{4\pi k}\left[-1-e^{-jk\mu_c}+e^{-jk\frac{2\pi}{3}}+e^{-jk(\mu_a+\frac{2\pi}{3})}\right]\left(1-e^{-jk\pi}\right)e^{-jk\left(\alpha+\frac{\pi}{6}-\varphi_{aP}\right)}e^{jk\frac{2\pi}{3}}$$

The results show that up to the third harmonic (3rd component) of the voltage switching functions are adequate for calculation of the second harmonic dc voltage mentioned in (5-15). However, it is possible to include higher factors as well if more accuracy is desired.

5.1.4 AC current switching functions

In this section the dynamic phasor equations of the ac current of a LCC operating under unbalanced conditions are derived. As explained in Chapter 4 the ac side current waveforms of the 6-pulse converter can be expressed in terms of the dc-side current and their current switching functions as follows.

$$i_a = f_{iaU}\, i_d$$

$$i_b = f_{ibU}\, i_d \quad (5\text{-}17)$$

$$i_c = f_{icU}\, i_d$$

where f_{iaU}, f_{ibU} and f_{icU} are the current switching functions of a LCC operating under unbalanced conditions for phases a, b, and c respectively. The functions f_{vaU}, f_{vbU} and f_{vcU} are shown in Figure 5-3. Similar to balanced operating conditions the trapezoidal approximation method has been used.

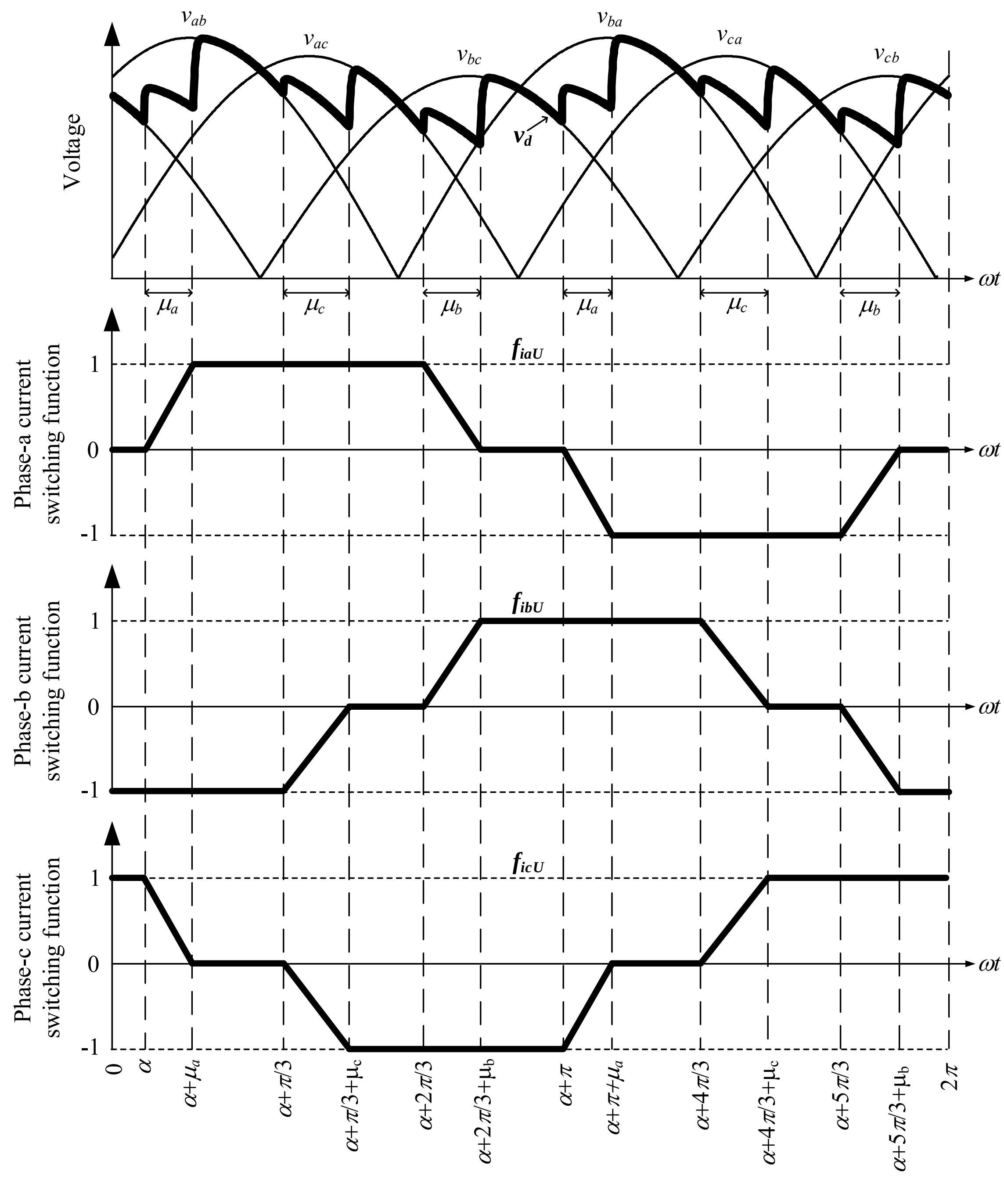

Figure 5-3: Current switching functions of phases a, b, and c for unbalanced condition. The DC side voltage of the LCC is also showed at the top waveform.

The fundamental component of the ac current is calculated using (5-17). However, as discussed in Chapter 4 it possible to add other harmonics if so desired. The fundamental frequency component of phases a, b, and c are calculated by applying (2-2) to (5-17).

$$\begin{aligned}
\langle i_a \rangle_1 &= \langle f_{iaU}\, i_d \rangle_1 \\
\langle i_b \rangle_1 &= \langle f_{ibU}\, i_d \rangle_1 \\
\langle i_c \rangle_1 &= \langle f_{icU}\, i_d \rangle_1
\end{aligned} \tag{5-18}$$

The right-hand side of the above equation can be expanded as follows:

$$\begin{aligned}
\langle i_a \rangle_1 &= \langle f_{iaU} \rangle_1 \langle i_d \rangle_0 + \langle f_{iaU} \rangle_3 \langle i_d \rangle_{-2} + \langle f_{iaU} \rangle_{-1} \langle i_d \rangle_2 \\
\langle i_b \rangle_1 &= \langle f_{ibU} \rangle_1 \langle i_d \rangle_0 + \langle f_{ibU} \rangle_3 \langle i_d \rangle_{-2} + \langle f_{ibU} \rangle_{-1} \langle i_d \rangle_2 \\
\langle i_c \rangle_1 &= \langle f_{icU} \rangle_1 \langle i_d \rangle_0 + \langle f_{icU} \rangle_3 \langle i_d \rangle_{-2} + \langle f_{icU} \rangle_{-1} \langle i_d \rangle_2
\end{aligned} \tag{5-19}$$

As mentioned in the previous section it is known that in the presence of unbalanced ac voltages in a LCC the dc voltage of the converter will have a second harmonic component in addition to the dc component. This will result in the presence of second harmonic in the dc current as well. Therefore, to develop the dynamic phasor equations of the ac current for a LCC operating under unbalanced conditions both the zero- and second-order components of the dc current are considered.

To obtain the right-hand side of the (5-19) it is necessary to determine the 1st and 3rd factor of current switching function. The k^{th} factors of current switching functions are as follows.

$$\left\langle f_{iaU}\right\rangle_k = \frac{j}{2\pi k^2}\left[\frac{1}{\mu_a}\left(e^{-jk\mu_a}-1\right)+\frac{1}{\mu_b}\left(1-e^{-jk\mu_b}\right)e^{-jk\frac{2\pi}{3}}\right]\left(1-e^{-jk\pi}\right)e^{-jk\left(\alpha+\frac{\pi}{6}-\varphi_{aP}\right)}$$

$$\left\langle f_{ibU}\right\rangle_k = \frac{j}{2\pi k^2}\left[\frac{1}{\mu_b}\left(e^{-jk\mu_b}-1\right)+\frac{1}{\mu_c}\left(1-e^{-jk\mu_c}\right)e^{-jk\frac{2\pi}{3}}\right]\left(1-e^{-jk\pi}\right)e^{-jk\left(\alpha+\frac{\pi}{6}-\varphi_{aP}\right)}e^{-jk\frac{2\pi}{3}} \tag{5-20}$$

$$\left\langle f_{icU}\right\rangle_k = \frac{j}{2\pi k^2}\left[\frac{1}{\mu_c}\left(e^{-jk\mu_c}-1\right)+\frac{1}{\mu_a}\left(1-e^{-jk\mu_a}\right)e^{-jk\frac{2\pi}{3}}\right]\left(1-e^{-jk\pi}\right)e^{-jk\left(\alpha+\frac{\pi}{6}-\varphi_{aP}\right)}e^{jk\frac{2\pi}{3}}$$

The terms $\langle i_d\rangle_0$ and $\langle i_d\rangle_{-2}$ in (5-19) are calculated in a similar way to the dc system equations developed in Chapter 4, in which the dynamic equations of the dc transmission line were developed. In the next section the dynamic phasor equations of the dc system will be developed for a LCC-HVDC transmission systems operating under unbalanced conditions.

5.1.5 DC system expressions

In this section the dynamic phasors model of the dc system is developed for a LCC-HVDC operating under unbalanced conditions. For the convenience of readers, the time-domain equations of the dc system are shown again as follows.

$$\begin{aligned}
\frac{di_{dR}}{dt} &= \frac{1}{L_{dynR}}(v_{dR}-v_c-\frac{R_d}{2}i_{dR}) \\
\frac{di_{dI}}{dt} &= \frac{1}{L_{dynI}}(v_c-v_{dI}-\frac{R_d}{2}i_{dI}) \\
\frac{dv_c}{dt} &= \frac{1}{C}(i_{dR}-i_{dI})
\end{aligned} \tag{5-21}$$

The dynamic phasor equivalents of these equations are obtained using (2-2) with k=0 (to denote the dc component) and k=2 (to denote the second harmonic component). The resulting equations are as follows.

$$\begin{aligned}
\frac{d\langle i_{dR}\rangle_0}{dt} &= \frac{1}{L_{dynR}}\left(\langle v_{dR}\rangle_0 - \langle v_c\rangle_0 - \frac{R_d}{2}\langle i_{dR}\rangle_0\right) \\
\frac{d\langle i_{dI}\rangle_0}{dt} &= \frac{1}{L_{dynR}}\left(\langle v_c\rangle_0 - \langle v_{dI}\rangle_0 - \frac{R_d}{2}\langle i_{dI}\rangle_0\right) \\
\frac{d\langle v_c\rangle_0}{dt} &= \frac{1}{C}\left(\langle i_{dR}\rangle_0 - \langle i_{dI}\rangle_0\right)
\end{aligned} \tag{5-22}$$

$$\begin{aligned}
\frac{d\langle i_{dR}\rangle_2}{dt} &= \frac{1}{L_{dynR}}\left(\langle v_{dR}\rangle_2 - \langle v_c\rangle_2 - \frac{R_d}{2}\langle i_{dR}\rangle_2\right) - j2\omega_s\langle i_{dR}\rangle_2 \\
\frac{d\langle i_{dI}\rangle_2}{dt} &= \frac{1}{L_{dynR}}\left(\langle v_c\rangle_2 - \langle v_{dI}\rangle_2 - \frac{R_d}{2}\langle i_{dI}\rangle_2\right) - j2\omega_s\langle i_{dI}\rangle_2 \\
\frac{d\langle v_c\rangle_2}{dt} &= \frac{1}{C}\left(\langle i_{dR}\rangle_2 - \langle i_{dI}\rangle_2\right) - j2\omega_s\langle v_c\rangle_2
\end{aligned} \tag{5-23}$$

As mentioned before in the properties of dynamic phasors the negative factors in (2-2) can be calculated by calculating the complex conjugates of the positive factors. Therefore the negative factors in (5-19) can be calculated as follows.

$$\begin{aligned}
\langle i_{dR}\rangle_{-2} &= \langle i_{dR}\rangle_2^* \\
\langle i_{dI}\rangle_{-2} &= \langle i_{dI}\rangle_2^* \\
\langle v_c\rangle_{-2} &= \langle v_c\rangle_2^*
\end{aligned} \tag{5-24}$$

5.1.6 YΔ transformers

In the above sections the dynamic phasors equations of a LCC operating under unbalanced conditions were developed. It was shown that the phase angle difference between positive sequence and negative sequence of the ac voltage is an key factor for developing of voltage and current switching functions for phases a, b, and c.

If a LCC is connected to a YY transformer, then the phase angle difference between the positive and negative sequence components will be the same for both primary and secondary side of the transformer. However, in case of a YΔ transformer if the phase angle difference between positive and negative sequence components is φ at the Y side of the transformer then the phase angle between positive and negative sequence voltage components will be $\varphi - \frac{\pi}{3}$.

Figure 5-4 shows an example of the phasor diagrams of line-to-ground and line-to-line voltages of balanced and unbalanced voltages. It can be observed that the phase angle between the negative and positive sequence of phase-a line-to-ground voltages is φ. However, the phase angle between the negative and positive sequence of line-to-line voltages (phase a and b) is $\varphi - \frac{\pi}{3}$.

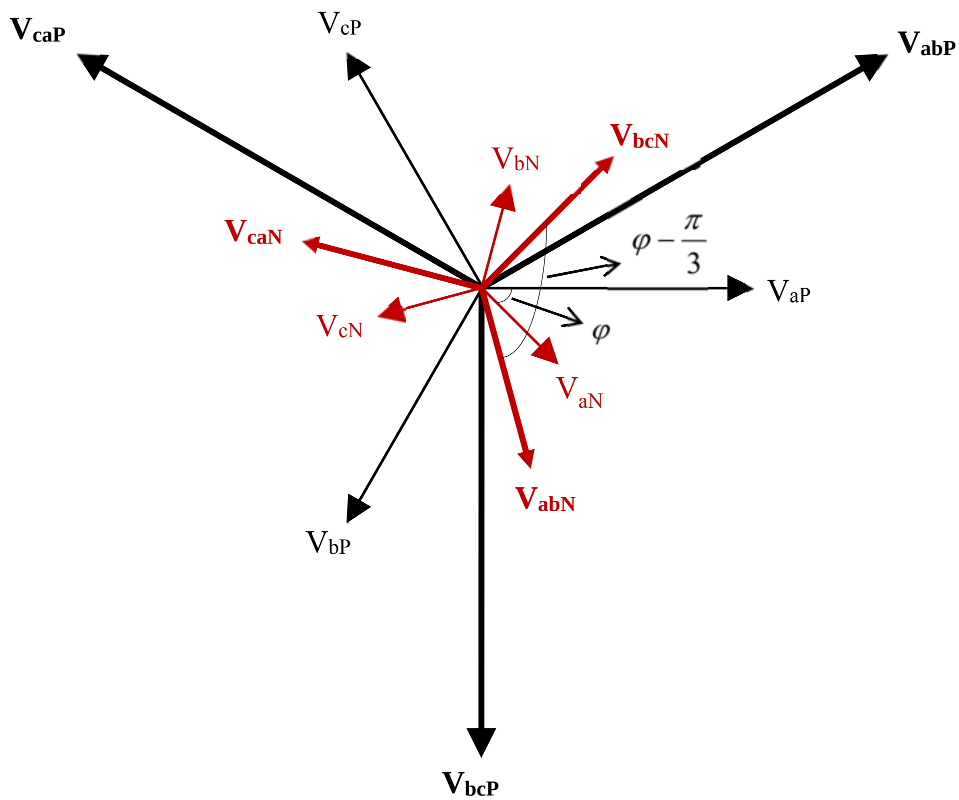

Figure 5-4: Phasor diagrams of balanced and unbalanced voltages.

5.1.7 Simulation results

In the above sections the dynamic phasors model of a LCC-HVDC operating under unbalanced conditions were developed. In this section the developed model is validated against the detailed model in PSCAD/EMTDC during several unbalanced conditions including unbalanced faults. Please note that the test system is exactly the same as the one discussed in previous chapter. System parameters and other specifications are shown in Appendix A.

Figure 5-5 shows the voltage and current waveforms of the converter for 50% unbalanced conditions (K=0.5). It can be seen that both the voltage and current of the dc side include second-order harmonic components, which is related to the unbalanced ac voltages. The results show that the developed dynamic phasor model can accurately capture the second harmonic components caused by unbalanced ac voltages.

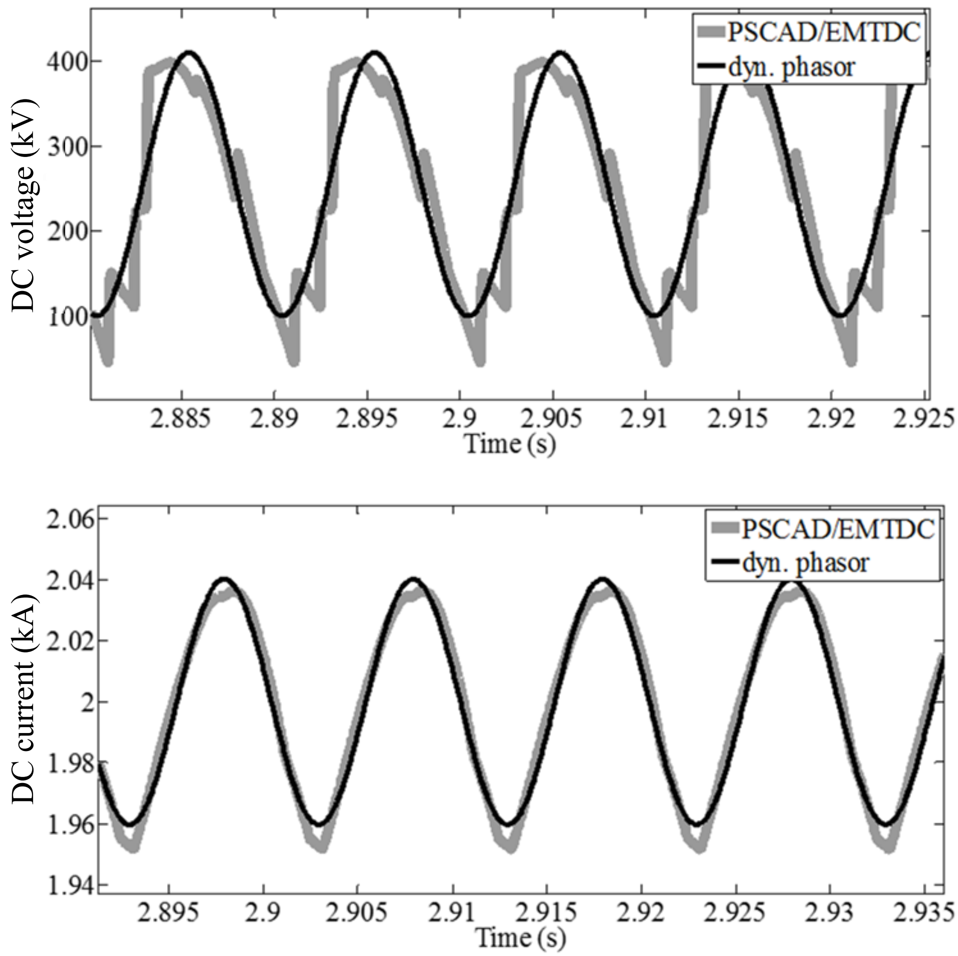

Figure 5-5: DC voltage (top) and DC current (bottom) of the converter for 50% unbalanced conditions (K=0.5).

Figure 5-6 shows the results of both voltage and current of the converter for an unbalanced fault, which results in 20% negative sequence component (K=0.2) and reduction of positive sequence voltage by 10%. It is clear from both the dynamic and steady state results that the developed model is able to properly model the system for both transients and steady state conditions.

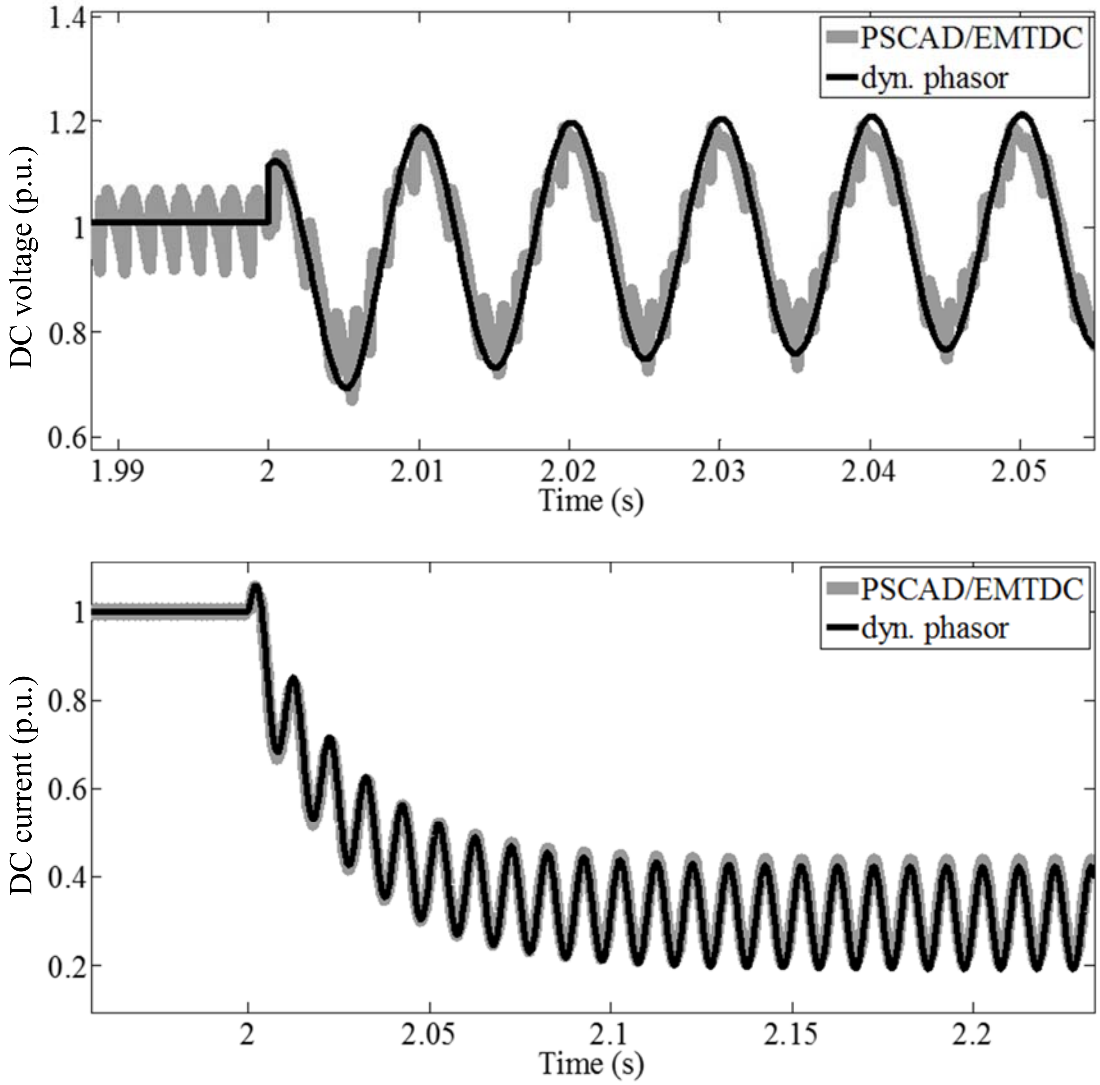

Figure 5-6: DC voltage (top) and DC current (bottom) of the converter for an unbalanced fault, which results in 20% negative sequence component (K=0.2) and reduction of positive sequence voltage by 10%.

In this section the dynamic phasor model of LCC HVDC transmission systems operating under unbalanced conditions were developed. This is, in particular, advantageous for analyzing the system under unbalanced faults. The developed model was validated against first CIGRE HVDC test system and it was shown that the developed model is capable of properly simulating the system under unbalanced operating conditions for both steady state and dynamic conditions.

5.2 Commutation Failure

In the previous chapter the dynamic phasor model of a LCC-HVDC transmission system operating under balanced conditions were developed. The derived model was validated against the results of a PSCAD/EMTDC model and it was shown that the model is accurate in capturing both transient and steady state results. It was, however, observed that the developed model din not properly simulate the system during commutation period.

In this section it is intended to modify and extend the model in order to be able to properly capture the transient of the system during commutation period. For the convenience of readers, the equivalent circuit of a LCC during commutation failure is shown again in Figure 5-7.

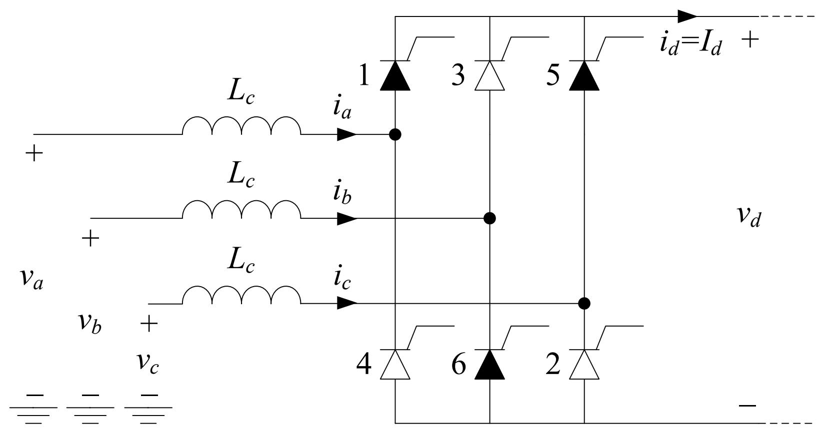

Figure 5-7: Equivalent circuit of the LCC during commutation (valves 1 and 5).

The first step to model a LCC operating during commutation failure is to detect when commutation failure is about to happen. With such information it is possible to modify the dynamic phasor equations as soon as commutation failure is detected. After detecting the commutation failure, a new set of equations need to be used in order to properly model the system during this transient. As mentioned in Chapter 3, the DC current can be expressed as follows.

$$I_d = \frac{\sqrt{3}V_m}{2\omega L_c}\left(\cos\alpha - \cos(\alpha+\mu)\right) \tag{5-25}$$

It is obvious that the term $\cos(\alpha+\mu)$ is always equal or greater than -1. Therefore, in order to have successful commutation (no commutation failure) the following condition needs to be satisfied.

$$I_d \le \frac{\sqrt{3}V_m}{2\omega L_c}\left(\cos\alpha + 1\right) \tag{5-26}$$

If the above criterion is not met, then it is concluded that the system is under commutation failure. After detecting the commutation failure, it is now necessary to model the system under this operating regime. During commutation failure the commutation period between two valves becomes so long that the next commutation starts before the existing one ends. As an example of commutation failure, the commutation between valve 2 and valve 6 starts while the commutation between valve 1 and valve 5 is in progress. This causes the valves 2 and valve 5 conduct at the same time as shown in Figure 5-8.

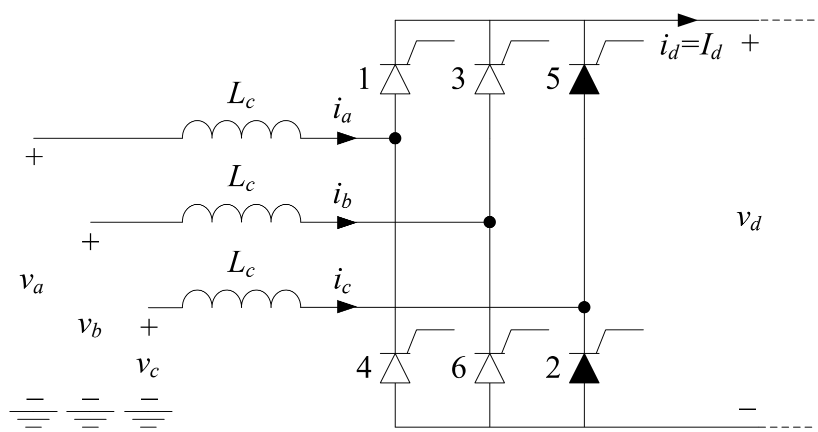

Figure 5-8: Equivalent circuit of the LCC during commutation failure

As it can be seen in the above figure during commutation failure the DC voltage become zero as valve 5 and valve 2 are both conducting. The AC current also becomes zero meaning that AC side becomes isolated from the DC side. Therefore, during commutation period, the following equations are valid.

$$v_d = 0$$

$$\begin{cases} i_a = 0 \\ i_b = 0 \\ i_c = 0 \end{cases} \tag{5-27}$$

Figure 5-9 shows the results of both rectifier and inverter current for a 10% reduction in the inverter's AC voltage, which causes commutation failure in the inverter side. In Figure 5-9 the results of the developed dynamic phasor model both with and without commutation failure modification of the dynamic phasor model are compared with the results of PSCAD/EMTDC.

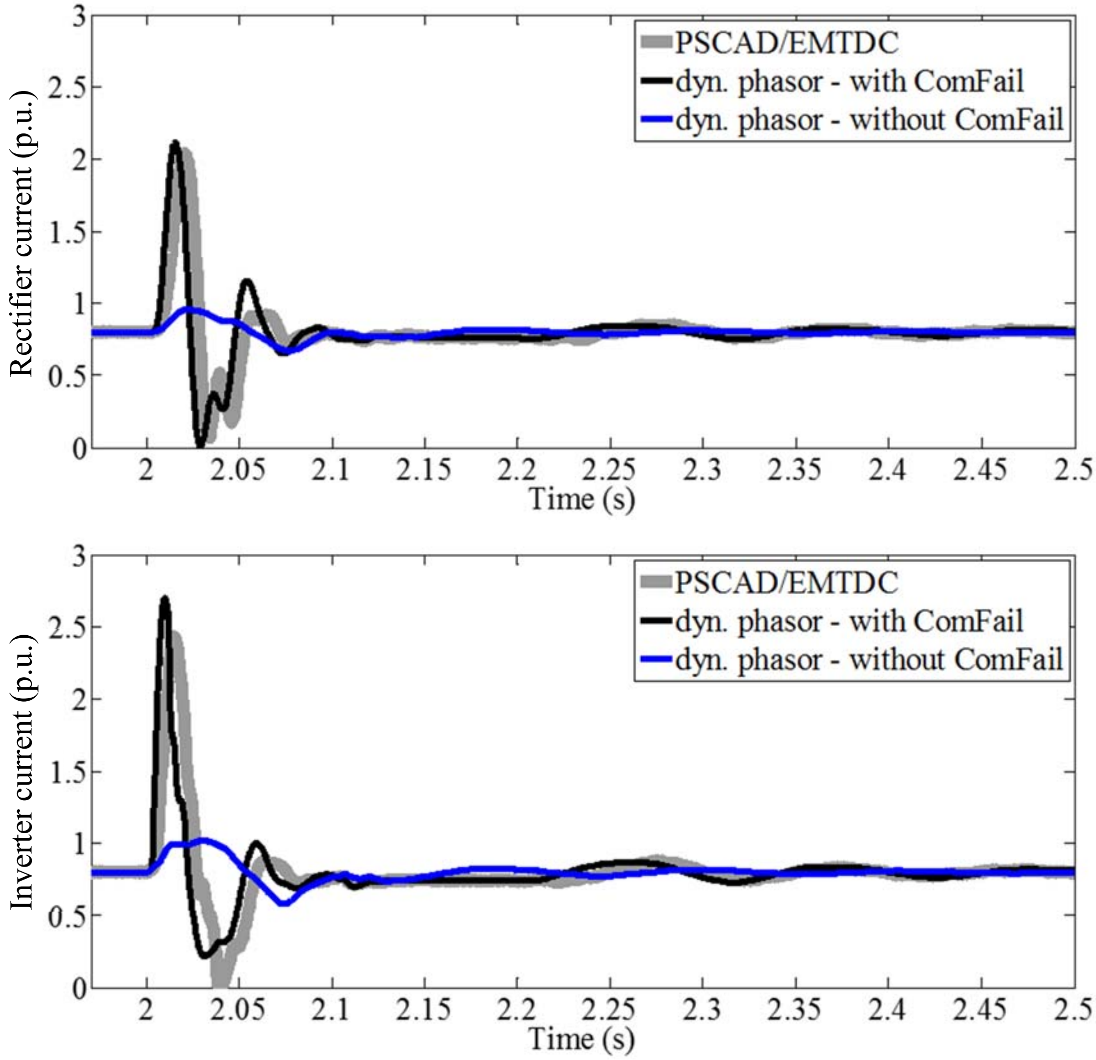

Figure 5-9: Rectifier (top) and inverter (bottom) current during commutation failure

5.3 Chapter Summary

In this chapter the developed dynamic phasor model in Chapter 4 was further developed in order to properly model both transient and the steady state response of the system during unbalanced conditions as well as operations under commutations failures. The model of a line-commutated converter operating under unbalanced conditions was first developed and then it was shown how to include the effect of a YΔ transformer to be able to expand the LCC model to a 12-brige converter of CIGRE first HVDC benchmark system.

With the improvements done in this chapter and their verification via comparison with EMT simulation results it is concluded that the developed model is able to fully model the LCC-based HVDC transmission systems during both transients and steady state for various operating conditions.

Chapter 6

Conclusions, Contributions, and Future Work

6.1 Conclusions and Contributions

High-voltage direct current power transmission systems are becoming increasingly integrated into modern power networks. The majority of HVDC transmission systems in the world are based upon line-commutated converters.

Computer simulations have been a significant part of control, design, and operation of power systems for many years. Different computer simulation programs have been developed for different types of studies in power systems. Among them, electromagnetic transient (EMT) programs are the most accurate one and use the most detailed models of the power system components, which make EMT simulation slow. Therefore, EMT programs are traditionally considered to be suitable only for small networks or studies with the short periods of interest. However, because of the complexity and interconnectivity of the modern power networks, it is necessary to use EMT programs for both larger networks and longer durations of time. Therefore, research needs to be done to develop both new simulation techniques and new models for power system components to accomplish this goal. The conclusions and contributions of the thesis are described as below:

1. *Development of a switching function-based model of a LCC-HVDC system*

The thesis developed the dynamic phasor model of a LCC bridge using the concept of switching functions. This model facilitates the analysis of the LCC and has the capability to be used to model the LCC for high-order harmonics and operating under unbalanced conditions and commutation failure.

The developed model was shown to be accurate in predicting the transient and steady-state large-signal response of the system over a frequency range that well exceeds the fundamental frequency of the variables of interest. This expanded range is unattainable by constant-admittance matrix models. The dynamic phasor model is, therefore, deemed an acceptably accurate and computationally inexpensive option for the analysis of the dynamic behaviour of an LCC-HVDC system and for the study of interactions between ac and dc systems.

2. *Analysis of waveform approximation for the AC current of a LCC*

In the thesis an investigation was done on the error introduced by the square-wave approximation of the AC current of a LCC (both magnitude and phase angle) and it was shown that this error can be large. Therefore, a trapezoidal-wave approximation was adopted and it was shown that this method is more accurate while the formula is still simple enough to be used in dynamic phasor model.

3. *Inclusion of high-order harmonics*

The developed model has the capability of including any number of harmonics in addition to the fundamental frequency component, albeit at the expense of a higher order model.

This can be helpful in the case one is interested to observe the effect of specific harmonic(s) separately. This can also be beneficial in controller design as the user has access to each and every harmonic independently.

4. *Operating under unbalanced conditions*

The developed model was further expanded to accurately model a LCC-HVDC under unbalanced condition. This is essential in order to investigate the dynamic behaviour of the system under unbalanced operating conditions of the system such as single-phase-to-ground (which is the most common fault in power systems) and double-phase-to-ground faults.

5. *Commutation failure*

The developed model would not be complete unless the model is able to properly represent a LCC-HVDC system operating during commutation failure as this is crucial for investigating dynamics of the system under sever faults causing commutation failures. The model was expanded to properly represent the system under this phenomenon.

6.1.1 Publications arising from the thesis

- M. Daryabak, S. Filizadeh, J. Jatskevich, A. Davoudi, M. Saeedifard, V. K. Sood, J. A. Martinez, D. Aliprantis, J. Cano, A. Mehrizi-Sani, "Modeling of LCC-HVDC Systems Using Dynamic Phasors," *IEEE Transaction on Power Delivery,* vol. 29, no. 4, pp. 721-726, Aug 2014. [55]

This paper presents an average-value model of a line commutated converter-based HVDC system using dynamic phasors. The model represents the low-frequency dynamics of the converter and its ac and dc systems, and has lower computational requirements than a conventional electromagnetic transient (EMT) switching model. The developed dynamic-phasor model is verified against an EMT model of the CIGRE HVDC Benchmark. Simulation results confirm the validity and accuracy of the average-value model in predicting the low-frequency dynamics of both the ac and dc side quantities. Merits and applicability limitations of the average model are highlighted.

- M. Daryabak, S. Filizadeh, "Analysis of Waveform Approximation for the AC Current of a Line-Commutated Converter," in *The 3rd International Conference on Electric Power and Energy Conversion Systems (EPECS)*, Istanbul, 2013. [56]

This paper analyzes mathematical approximations of the ac current of a line-commutated converter (LCC), which is the building block of conventional HVDC systems. The paper derives analytical expressions for the ac current of an LCC during the commutation and non-commutation periods and continues with calculating the percentage error of both the fundamental frequency component of the ac current and the power factor of the converter when the ac current is approximated with either a square or a trapezoidal waveform. The results quantitatively show the benefit of the trapezoidal waveform approximation in terms of its percentage error and simplicity.

6.2 Directions for Future Work

The developed model in this research is in dynamic phasor format and domain. It is recommended to perform research in order to find methods on how to integrate this model in electromagnetic transient programs. This can also be advantageous in using the developed model in existing electromagnetic transient programs.

It is also recommended to develop a systematic way to assemble network and converter equations. This will be helpful in integration of the dynamic phasor model of LCC-HVDC with any AC network regardless of the complexity of the ac system and its interconnections.

A proper and formal analysis of computational savings in terms of computing time and simulation time step also is recommended for future investigation. Such an analysis will firmly quantify the computational benefits of simulating with dynamic phasors.

Bibliography

[1] E. W. Kimbark, Direct Current Transmission, Wiley, 1971.

[2] V. K. Sood, HVDC and FACTS Controllers - Applications of Static Converters in Power Systems, Kluwer Academic Publishers, 2004.

[3] M. P. Bahrman, B. Johnson, "The ABCs of HVDC transmission technologies," *IEEE Power and Energy Magazine,* vol. 5, no. 2, pp. 32-44, April 2007.

[4] S. Henschel, "Analysis of electromagnetic and electromechanical power system transients with dynamic phasors," Ph. D. dissertation, Dept. Elect. & Com. Eng., University of British Columbia, Vancouver, 1999.

[5] M. Faruque, Y. Zhang, and V. Dinavahi, "Detailed modeling of CIGRE HVDC benchmark system using PSCAD/EMTDC and PSB/SIMULINK," *IEEE Trans. on Power Delivery,* vol. 21, no. 1, pp. 378-387, January 2006.

[6] S. Filizadeh, A. M. Gole, D. A. Woodford, and G. D. Irwin, "An optimization-enabled electromagnetic transient simulation-based methodology for HVDC controller design," *IEEE Trans. on Power Delivery,* vol. 22, no. 4, pp. 2559-2566, Oct 2007.

[7] V. K. Sood, V. Khatri, H. Jin, "EMTP modeling of CIGRE benchmark based HVDC transmission system operating with weak ac systems," in *IEEE Int'l Conf. on Power Electronics, Drives and Energy Systems for Industrial Growth*, New Delhi, India, 1996.

[8] B. Gemmell and J. Laughran, "HVDC offers the key to untapped hydro," *IEEE Power Eng. Rev.,* vol. 22, no. 5, pp. 8-11, May 2002.

[9] C. Karawita and U. Annakkage, "Multi-in-feed HVDC interaction studies using small signal stability assessment," *IEEE Trans. on Power Delivery,* vol. 24, no. 2, pp. 910-918, Apr 2009.

[10] S. R. Sanders, J. M. Noworolski, X. Z. Liu, and G. C. Verghese, "Generalized averaging method for power conversion circuits," *IEEE Trans. on Power Electronics,* vol. 6, no. 2, pp. 251-259, April 1991.

[11] A. Yazdani and R. Iravani, "A generalized state-space averaged model of the three-level NPC converter for systematic dc-voltage-balancer and current-controller design," *IEEE Trans. on Power Delivery,* vol. 20, pp. 1105-1114, Apr 2005.

[12] A. Stankovic, B. Lesieutre, and T. Aydin, "Modeling and analysis of single-phase induction machines with dynamic phasors," *IEEE Trans. on Power Systems,* vol. 14, no. 1, pp. 9-14, Feb 1999.

[13] A. M. Stankovic, S. R. Sanders, and T. Aydin, "Dynamic phasors in modeling and analysis of unbalanced polyphase AC machines," *IEEE Trans. on Energy Conversion,* vol. 17, no. 1, pp. 107-113, March 2002.

[14] A. M. Stankovic, B. Lesieutre, T. Aydin, "Applications of generalized averaging to synchronous and induction machines," in *in Proc. North American Power Symposium*, B. Lesieutre, 1996.

[15] A. M. Stankovic and T. Aydin, "Analysis of asymmetrical faults in power systems using dynamic phasors," *IEEE Trans. on Power Systems,* vol. 15, no. 3, pp. 1062-1068, Aug 2000.

[16] T. H. Demiray, "Simulation of power system dynamics using dynamic phasor models," Ph. D. dissertation, Swiss Federal Institute of Technology, Zurich, 2008.

[17] P. Mattavelli, G. C. Verghes e, and A. M. Stankovic, "Phasor dynamics of thyristor-controlled series capacitor systems," *IEEE Trans. on Power Systems,* vol. 12, no. 3, pp. 1259-1267, Aug 1997.

[18] P. C. Stefanov and A. M. Stankovic, "Modeling of UPFC operation under unbalanced conditions with dynamic phasors," *IEEE Trans. on Power Systems,* vol. 17, no. 2, pp. 395-403, May 2002.

[19] P. Mattavelli, A. M. Stankovic, and G. C. Verghese, "SSR analysis with dynamic phasor model of thyristor-controlled series capacitor," *IEEE Trans. on Power Systems,* vol. 14, no. 1, pp. 200-208, Feb 1999.

[20] V. A. Caliskan, O. C. Verghese, A. M. Stankovic, "Multifrequency averaging of dc-dc converters," *IEEE Trans. Power Electronics,* vol. 14, pp. 124-133, Jan 1999.

[21] A. Emadi, "Modeling and analysis of multiconverter DC power electronic systems using the generalized state-space averaging method," *IEEE Trans. Industrial Electronics,* vol. 51, pp. 661-668, June 2004.

[22] A. Emadi, "Modeling of power electronics loads in AC distribution systems using the generalized state-space averaging method," *IEEE Trans. Industrial Electronics,* vol. 51, pp. 992-1000, Oct 2004.

[23] S. Chandrasekar, R. Gokaraju, "Dynamic Phasor Modeling of Type 3 DFIG Wind Generators (Including SSCI Phenomenon) for Short-Circuit Calculations," *IEEE Transactions on Power Delivery,* vol. 30, no. 2, pp. 887-897, 2015.

[24] A. Gole, S. Filizadeh, R. Menzies, and P. Wilson, "Optimization-enabled electromagnetic transient simulation," *IEEE Trans. on Power Delivery,* vol. 20, no. 1, pp. 512-518, Jan 2005.

[25] H. Duchen, M. Lagerkvist, R. Kuffel, and R. Wierckx, "HVDC simulation and control system testing using a real-time digital simulator (RTDS)," in *Proc. first international conference on digital power system simulators*, 1995.

[26] W. Hammer, "Dynamic modeling of line and capacitor commutated converters for HVDC power transmission," Ph. D. dissertation, Swiss Federal Institute of Technology, Zurich, 2003.

[27] M. Szechtman, T. Wess, and C. V. Thio, "First benchmark model for HVDC control studies," *Electra,* vol. 135, pp. 55-75, Apr 1991.

[28] P. M. Anderson, B. L Ageawal, J. E. Van Ness, Sub-synchronous Resonance in Power Systems, New York: IEEE PRESS, 1990.

[29] Douglas L. Elkins, Avi C. Jain, Thomas E. McDermott, and Volker Rees, "Transients During 138-kV SF6 BreakerSwitching of Low Inductive Currents," *IEEE Transaction on Industry Application,* vol. 29, no. 4, pp. 721-726, July/August 1993.

[30] R. Mahmutcehajic, S. Babic, R. Garcanovic, S. Carsimamovic, "Digital simulation of electromagnetic wave propagation in a multiconductor transmission system using

the superposition principle and Hartley transform," *IEEE Transaction on Power Delivery,* vol. 8, no. 3, pp. 1377-1385, July 1993.

[31] R.B. Rodrigues, V.M.F. Mendes, J.P.S Catalao, "Electromagnetic transients due to lightning strikes on wind turbines: A case study," in *2010 15th IEEE Mediterranean Electrotechnical Conference*, Valletta, 2010.

[32] D.T.A. Kho, M.D. Greenwood, K.S. Smith, "Analysis of switching over-voltages in a three-ended 400 kV cable system," in *2009 Proceedings of the 44th International Universities Power Engineering Conference (UPEC)*, Glasgow, 2009.

[33] A. Bayadi, N. Harid, K. Zehar, S. Belkhiat, "Simulation of metal oxide surge arrester dynamic behavior under fast transients," in *The international Conference on Power Systems Transients - IPST*, New Orleans, USA, 2003.

[34] H.W. Dommel, A. Yan, S. Wei, "Harmonics from Transformer Saturation," *IEEE Transaction on Power Delivery,* pp. 209-215, April 1986.

[35] A. D. Rajapakse, A. M. Gole, R. P. Jayasinghe, "An Improved Representation of FACTS Controller Semiconductor Losses in EMTP-Type Programs Using Accurate Loss-Power Injection Into Network Solution," *IEEE Transactions on Power Delivery,* vol. 24, no. 1, pp. 381-389, Jan 2009.

[36] M. Elfayoumy, C.G. Moran, "A comprehensive approach for subsynchronous resonance screening analysis using frequency scanning technique," in *Power Tech Conference Proceedings*, Bologna, 2003.

[37] "Comparison of transient stability analysis and large-scale real time digital simulation," in *2001 IEEE Porto Power Tech Proceedings*, Porto, 2001.

[38] J.M. Mauricio, A. Marano, A. Gomez-Exposito, J.L. Martinez Ramos, "Frequency Regulation Contribution Through Variable-Speed Wind Energy Conversion Systems," *IEEE Transaction on Power Systems,* vol. 24, no. 1, pp. 173-180, Feb 2009.

[39] E. Vaahedi, L, Wenyuan, T. Chia, H. Dommel, "Large scale probabilistic transient stability assessment using BC Hydro's on-line tool," *IEEE Transaction on Power Systems,* vol. 15, no. 2, pp. 661-667, May 2000.

[40] K. R. Padiyar, HVDC power transmission systems: technology and system interactions, John Wiley & Sons, 1990.

[41] M. Kulasza, "Generalized Dynamic Phasor-Based Simulation for Power Systems," M.Sc. thesis, Dept. Elec. & Com. Eng. University of Manitoba, Winnipeg, 2014.

[42] O. Anaya-Lara, D. Campos-Gaona, E. Moreno-Goytia, G. Adam, Offshore Wind Energy Generation: Control, Protection, and Integration to Electrical Systems, WILEY, 2014.

[43] Q. Qi, L. Jiao, Z. Yan, Y. Ni, S. Chen, and F. Wu, "Modeling and simulation of HVDC with dynamic phasors," in *in proc. of the CSEE*, 2003.

[44] J. Arrillaga, Y.H. Liu, and N.R. Watson, Flexible Power Transmission: The HVDC Options, John Wiley & Sons, Ltd, 2007.

[45] L. Gyugyi and B. R. Pelly, Static Power Frequency Changers. - Theory, Performance, and application, Wiley, 1976.

[46] P. C. Krause, O.Wasynczuk, S. D. Sudhoff, Analysis of Electric Machinery and Drive Systems, Piscataway IEEE Press/Wiley, 2002.

[47] M. Parniani, M. R. Iravani, "Computer analysis of small signal stability of power systems including network dynamics," in *IEE Proc. Gener., Transm. Distrib.*, 1995.

[48] C. Osauskas, A. Wood, "Small-signal dynamic modeling of HVDC systems," *IEEE Trans. on Power Delivery,* vol. 18, no. 1, pp. 220-225, Jan 2003.

[49] J. D. Ainsworth, "The Phase-Locked Oscillator - A New Control System for Controlled Static Convertors," *IEEE Transaction on Power Apparatus,* Vols. PAS-87, no. 3, p. 859–865, March 1968.

[50] A. M. Gole, V. K. Sood, and L. Mootosamy, "Validation and Analysis of a Grid Control System Using D-Q-Z Transformation for Static compensator Systems," in *Canadian Conference on Electrical and Computer Engineering*, Montreal, 1989.

[51] D.A. Woodford, A.M. Gole, R.W. Menzies, "Digital Simulation of DC Links and AC Machines," *IEEE Transactions on Power Apparatus and Systems,* Vols. PAS-102, no. 6, pp. 1616-1623, June 1983.

[52] T.Ino, R.M.Mathur, M.R.Iravani and S.Sasaki, "Validation of Digital Simulation of DC Links - Part II," *IEEE Transactions on Power Apparatus and Systems,* Vols. PAS-104, no. 9, pp. 2596-2602, 1985.

[53] T.Ino, R.M.Mathur, M.R.Iravani and S.Sasaki, "Validation of Digital Simulation of DC Links - Part II," *IEEE Transactions on Power Apparatus and Systems,* Vols. PAS-104, no. 9, pp. 2596-2602, 1985.

[54] P. Kuffel, K.L. Kent, G.B. Mazur, M.A. Weekes, "Development and Validation of Detailed Controls Models of the Nelson River Bipole 1 HVDC System," *IEEE Transactions on Power Delivery,* vol. 8, no. 1, pp. 351-358, 1993.

[55] M. Daryabak, S. Filizadeh, J. Jatskevich, A. Davoudi, M. Saeedifard, V. K. Sood, J. A. Martinez, D. Aliprantis, J. Cano, A. Mehrizi-Sani, "Modeling of LCC-HVDC Systems Using Dynamic Phasors," *IEEE Transaction on Power Delivery,* vol. 29, no. 4, pp. 721-726, Aug 2014.

[56] M. Daryabak, S. Filizadeh, "Analysis of Waveform Approximation for the AC Current of a Line-Commutated Converter," in *The 3rd International Conference on Electric Power and Energy Conversion Systems (EPECS)*, Istanbul, 2013.